HAL
open science

Phytoplankton light absorption and the package effect in relation to photosynthetic and photoprotective pigments in the northern tip of Antarctic Peninsula

Amabile Ferreira, Aurea M. Ciotti, Carlos Rafael B. Mendes, Julia Uitz, Annick Bricaud

To cite this version:

Amabile Ferreira, Aurea M. Ciotti, Carlos Rafael B. Mendes, Julia Uitz, Annick Bricaud. Phytoplankton light absorption and the package effect in relation to photosynthetic and photoprotective pigments in the northern tip of Antarctic Peninsula. Journal of Geophysical Research. Oceans, 2017, 122 (9), pp.7344-7363. 10.1002/2017JC012964 . hal-03502951

HAL Id: hal-03502951

https://hal.science/hal-03502951v1

Submitted on 27 Dec 2021

HAL is a multi-disciplinary open access archive for the deposit and dissemination of scientific research documents, whether they are published or not. The documents may come from teaching and research institutions in France or abroad, or from public or private research centers.

L'archive ouverte pluridisciplinaire **HAL**, est destinée au dépôt et à la diffusion de documents scientifiques de niveau recherche, publiés ou non, émanant des établissements d'enseignement et de recherche français ou étrangers, des laboratoires publics ou privés.

Copyright

AGU PUBLICATIONS

JGR

Journal of Geophysical Research: Oceans

RESEARCH ARTICLE

10.1002/2017JC012964

Key Points:

- Variations in photosynthetic and photoprotective pigments are not discernible by changes in the chlorophyll-specific absorption of phytoplankton
- A cluster analysis identifies a regular increase in the degree of package effect of phytoplankton absorption
- A regular increase in the degree of package effect is associated with an increase of fucoxanthin and decrease of photoprotective pigments relative to chlorophyll *a*

Correspondence to:
A. Ferreira,
amabilefr@gmail.com

Citation:
Ferreira, A., Á. M. Ciotti, C. R. B. Mendes, J. Uitz, and A. Bricaud (2017), Phytoplankton light absorption and the package effect in relation to photosynthetic and photoprotective pigments in the northern tip of Antarctic Peninsula, *J. Geophys. Res. Oceans*, *122*, 7344–7363, doi:10.1002/2017JC012964.

Received 4 APR 2017
Accepted 9 AUG 2017
Accepted article online 25 AUG 2017
Published online 13 SEP 2017

© 2017. American Geophysical Union. All Rights Reserved.

Phytoplankton light absorption and the package effect in relation to photosynthetic and photoprotective pigments in the northern tip of Antarctic Peninsula

Amabile Ferreira[1], Áurea M. Ciotti[1], Carlos Rafael B. Mendes[2], Julia Uitz[3,4], and Annick Bricaud[3,4]

[1]Centro de Biologia Marinha, Universidade de São Paulo, São Sebastião, São Paulo, Brazil, [2]Instituto de Oceanografia, Universidade Federal do Rio Grande, Rio Grande, Rio Grande do Sul, Brazil, [3]Sorbonne Universités, UPMC-Université Paris-VI, UMR 7093, LOV, Observatoire Océanologique, Villefranche/Mer, France, [4]Centre National de la Recherche Scientifique, UMR 7093, LOV, Observatoire Océanologique, Villefranche/Mer, France

Abstract This study investigates the variability in the spectral absorption of phytoplankton in Antarctic waters. A large in situ data set comprising phytoplankton pigments and hyperspectral absorption was measured in the northern tip of Antarctic Peninsula during 2013 and 2014 summers at several depths. A proxy of package effect was estimated from the phytoplankton absorption spectra, independently of chlorophyll *a*. Variations in the concentration of photosynthetic and photoprotective pigments were discernible by changes in this metric but not in the chlorophyll *a* specific absorption coefficient of phytoplankton. The fucoxanthin to chlorophyll *a* ratio correlated positively to package effect due to an increase in cell size of phytoplankton (diatoms) and increasing fucoxanthin content per cell to maximize light harvesting in depth. The package effect was found to covary inversely with photoprotective pigments relative to chlorophyll *a*, partially due to their contribution to enhance absorption in the blue part of the spectrum. Using a cluster analysis (*k*-means algorithm) on the phytoplankton absorption spectra, we illustrate the capacity to identify a regular increase in the degree of package effect. This approach can be useful to classify the phytoplankton assemblages in Antarctic waters according to different degrees of pigment packaging, each one related to a specific pigment composition. Our results demonstrate the potential for this classification at different temporal and spatial scales from ocean color satellite data. This should improve our understanding of deviations in global bio-optical algorithms when applied to the Southern Ocean.

1. Introduction

It has long been assumed that phytoplankton in Antarctica is under chronic low light, compared to that of lower latitude communities, due to larger solar zenith angles, cloud cover, and deeper vertical mixing [*Mitchell and Holm-Hansen*, 1991; *Mitchell*, 1992]. Early works in the Southern Ocean reported low light chl *a*-specific (i.e., per unit of chlorophyll *a* concentration) particulate absorption and attenuation [*Mitchell and Holm-Hansen*, 1991], diffuse vertical attenuation [*Mitchell*, 1992], and phytoplankton absorption [*Sosik et al.*, 1992] in the Antarctic Peninsula. Low chl *a*-specific absorption coefficients of phytoplankton, $a^*_{ph}(\lambda)$ ($m^2\ mg^{-1}$) observed at low irradiances result from an increase of chlorophyll *a* per cell to increase light harvesting (pigment packaging in the sense of *Duysens* [1956]) and also from a decrease of the proportion of photoprotective carotenoid pigments which enhance the magnitude of $a^*_{ph}(\lambda)$ [*Mitchell*, 1992].

Consequences of low $a^*_{ph}(\lambda)$ include an increase in the remote sensing reflectance (especially in the blue part of the spectrum) and, in turn, an underestimation of chlorophyll *a* concentration retrieved by global standard ocean color algorithms in the Southern Ocean [*Mitchell and Holm-Hansen*, 1991; *Dierssen and Smith*, 2000; *Garcia et al.*, 2005, *Marrari et al.*, 2006; *Szeto et al.*, 2011; *Johnson et al.*, 2013]. Uncertainties in the chlorophyll algorithms in Antarctic waters were also associated with variations of phytoplankton taxonomic composition along a latitudinal gradient [*Johnson et al.*, 2013] and low backscattering coefficients in the green part of the spectrum at high chlorophyll *a* [*Dierssen and Smith*, 2000]. Hence, several regional chlorophyll algorithms for the Antarctic Peninsula have been proposed [e.g., *Mitchell and Holm-Hansen*, 1991; *Dierssen and Smith*, 2000; *Marrari et al.*, 2006; *Kahru and Mitchell*, 2010; *Szeto et al.*, 2011].

While absorption properties may be different for Antarctic waters, the phytoplankton absorption has not been extensively studied in the region [*Mitchell and Holm-Hansen*, 1991; *Sosik et al*., 1992; *Stambler et al*., 1997; *Stambler*, 2003; *Arrigo et al*., 1998; *Dierssen and Smith*, 2000; *Reynolds et al*., 2001]. Some of those studies evidenced that, as in most of the oceans, the phytoplankton absorption characteristics are dependent on the cell size, taxonomic, and pigment composition of phytoplankton and can resemble those in temperate waters [*Arrigo et al*., 1998; *Dierssen and Smith*, 2000].

Alderkamp et al. [2010] hypothesized that photodamage incurred during the high irradiance period of the vertical mixing cycle, rather than light limitation, controls phytoplankton growth in regions of the Southern Ocean with deep mixed layers. Vertical mixing imposes intense irradiance fluctuations, from relatively high irradiance near the water surface to complete darkness below the euphotic zone [*van de Poll et al*., 2009]. Indeed, recent studies reported the presence of photoprotective pigments of phytoplankton in response to large vertical mixing depths in different regions in Antarctica such as the African sector of the Southern Ocean [*Alderkamp et al*., 2010], the Drake passage [*Alderkamp et al*., 2011], the Amundsen Sea [*Alderkamp et al*., 2013], the Sub-Antarctic and Polar Frontal Zone [*Cheah et al*., 2013], around the Shetland Islands [*García-Muñoz et al*., 2014], and the Ross Sea [*Neale et al*., 2009, 2012]. Logically, the role of vertical mixing on photoprotection cannot be generalized for the entire Southern Ocean that includes open ocean and coastal areas with very different environmental and light conditions. Despite the observations of high proportion of pigments devoted to photoprotection of phytoplankton in the Southern Ocean, no study explicitly investigated the influence of photosynthetic and photoprotective pigments on both $a^*_{ph}(\lambda)$ and the spectral variability of the phytoplankton absorption coefficient, $a_{ph}(\lambda)$.

Using a large data set of phytoplankton pigments and spectral absorption determined by current state-of-the-art methodologies (HPLC and spectrophotometry with an integrating sphere) collected in the northern tip of the Antarctic Peninsula, we (i) investigate the effect of chlorophyll *a*, photosynthetic and photoprotective pigments on variations in $a^*_{ph}(\lambda)$; (ii) quantify the degree of package effect of the $a_{ph}(\lambda)$ spectra; and (iii) characterize the spectral variability and features in $a_{ph}(\lambda)$. For the second objective, a metric for pigment packaging was estimated from the $a_{ph}(\lambda)$ spectra, independently of chlorophyll *a* concentration. We anticipate that variations in the concentration of photosynthetic and photoprotective pigments were more discernible by changes in this metric than in $a^*_{ph}(\lambda)$.

2. Materials and Methods

2.1. Sampling

Data were collected during two oceanographic cruises in the northern tip of the Antarctic Peninsula in the austral summers of 2013 (14 February to 3 March) and 2014 (8–24 February). The study area covered the Gerlache Strait (GS), which separates the Palmer Archipelago from the Peninsula, the Bransfield Strait (BS), between the southern Shetland Islands and the Peninsula, and the northwestern Weddell Sea (NWW). In 2013, stations in NWW were performed as close as possible to the marginal ice zone to investigate the influence of ice melting on the phytoplankton community structure (outside of the scope of the present work). Summer 2013 showed an unusual ice extension in the Weddell Sea, pushed northward toward lower latitudes (http://earthobservatory.nasa.gov/). Twelve of the 29 stations performed in 2013 on the marginal ice zone in NWW were sampled in 2014 to compare the same geographical location near (2013) and far away from (2014) the sea ice. Therefore, some of the differences in the phytoplankton abundance and taxonomy in NWW between both years are likely associated with the distance to the ice zone.

Some of the stations sampled in the southeastern BS were not visited in 2014, and eight additional stations were performed near the Elephant Island (Figure 1). In 2014, two stations were visited in NWW distant to the main domain of sampling, i.e., near the coast and ice edge in NWW, to sample waters visually characterized by a very high transparency. This area will be denoted hereafter as NWW_{HT} ($_{HT}$ denotes "high transparency"). A total of 89 and 70 stations were sampled in 2013 and 2014, respectively (Figure 1).

The euphotic depth (Z_{eu}) is defined as the depth where the photosynthetically available radiation is 1% of that observed at surface. Z_{eu} varied from 34 to 117 m, with an identical average of 61 m for each cruise. At stations performed at night, Z_{eu} was estimated by an empirical relationship derived from measured Z_{eu} and chlorophyll *a* concentration, [Chl *a*], measured at 5 m for the stations performed during daylight ($\log_{10}(Z_{eu}) = -0.45 \times \log_{10}([\text{Chl } a]) + 1.79$; $R^2 = 0.72$; $p < 0.00001$; $N = 78$). A statistical relationship was also

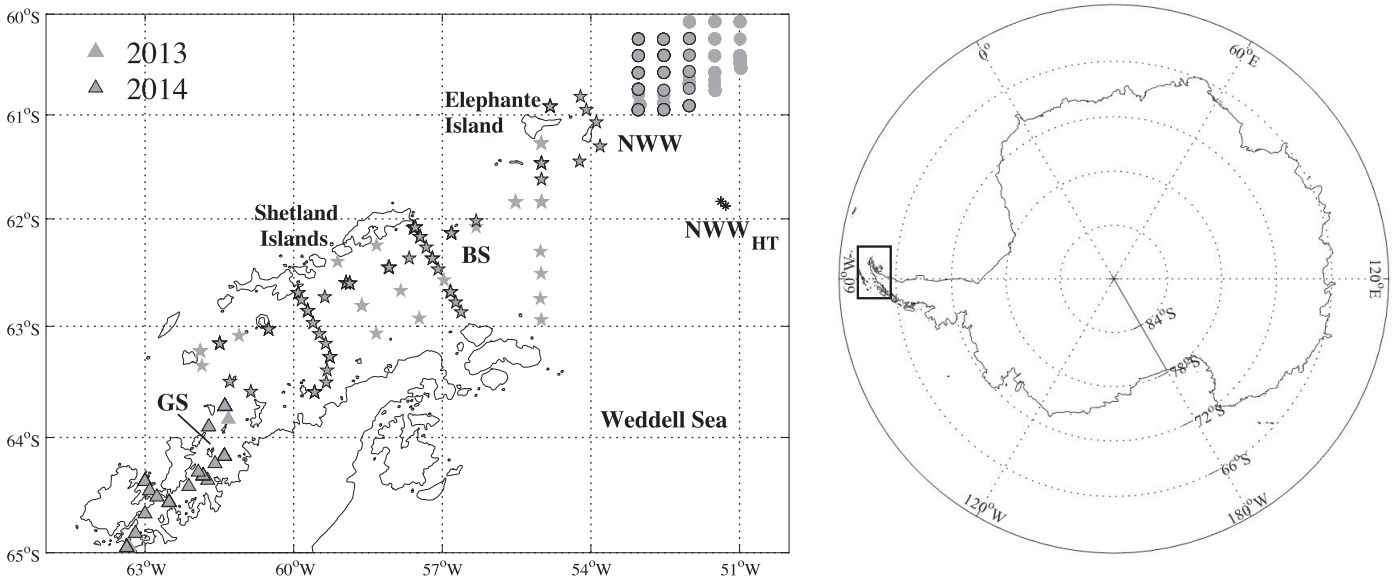

Figure 1. Geographic locations of the sampling stations in the Gerlache Strait (GS, triangles), Bransfield Strait (BS, stars), and northwestern Weddell Sea (NWW, circles). NWW_{HT} denotes "high transparency," with two stations sampled in 2014 (asterisks). In GS, BS, and NWW, most of the stations of 2013 were sampled in 2014 and are indicated with the edge markers in black.

established between Z_{eu} and [Chl *a*] integrated along the water column, but a lower significance was found compared to that considering [Chl *a*] at 5 m. The first optical depth, $Z_{37\%}$, at which the downward irradiance falls to 1/e (or 37%) of its value just below the surface, was obtained as Z_{eu} divided by 4.6 (=ln 100) [*Gordon and McCluney*, 1975; *Gordon and Morel*, 1983]. The depth where the downward irradiance falls to 10% of its value just below the surface was computed as Z_{eu} divided by 2.3 (=ln 10), $Z_{10\%}$. A number of 165 samples belonged to the layer between surface and $Z_{37\%}$, denoted as $L_{>37\%}$, and 98 samples were encountered between $Z_{37\%}$ and $Z_{10\%}$. This layer is denoted as $L_{37-10\%}$. A number of 281 samples were below $Z_{10\%}$, and this layer is hereafter referred as $L_{<10\%}$. The means of $Z_{37\%}$ and $Z_{10\%}$ were 12.83 and 25.67 m, respectively. Therefore, $L_{>37\%}$, $L_{37-10\%}$, and $L_{<10\%}$ comprised mostly samples at 5 m, 15 and 25 m, and 50–100 m, respectively. Note that many samples in $L_{<10\%}$ were below Z_{eu}.

2.2. HPLC Pigment Analysis

Concentrations of chlorophyll *a* and accessory pigments of phytoplankton were measured by high-performance liquid chromatography (HPLC), using the procedure described by *Mendes et al*. [2007, 2012]. For most of the stations, discrete water samples (1–2 L) were collected at 5, 15, 25, 50, 75, and 100 m. At stations performed during night, samples were collected only at 5 m. Samples were filtered onto 25 mm glass fiber filters (Whatman GF/F) for postcruise analysis.

The concentrations of monovinyl chlorophyll *a*, divinyl chlorophyll *a*, chlorophyll *a* epimers and allomers, chlorophyllide *a*, pheophytin *a*, and pheophorbide *a* were summed up and referred to as total chlorophyll *a* (denoted as [TChl *a*]). The degradation products of chlorophyll *a* were included in [TChl *a*] following *Bricaud et al*. [1995, 2004] to keep consistency for comparisons to *Bricaud et al*.'s studies. Note that the proportion of degradation products were low (means of 3, 3, and 6% in $L_{>37\%}$, $L_{37-10\%}$, and $L_{<10\%}$, respectively).

Accessory pigments determined by HPLC included: chlorophyll *b*; chlorophyll c_1, chlorophyll c_2, and chlorophyll c_3; prasinoxanthin, fucoxanthin, 19′-hexanoyloxyfucoxanthin, 19′-butanoyloxyfucoxanthin, peridinin, diadinoxanthin, diatoxanthin, alloxanthin, zeaxanthin, β-carotene, and α-carotene. We grouped the accessory pigments into photosynthetic carotenoids (denoted as PSC), consisting of fucoxanthin, 19′-hexanoyloxyfucoxanthin, 19′-butanoyloxyfucoxanthin, peridinin, prasinoxanthin, and α-carotene; and photoprotective carotenoids (denoted as PPC), consisting of alloxanthin, diadinoxanthin, diatoxanthin, zeaxanthin, and β-carotene. The photosynthetic pigment concentration, [PSC], was primarily determined by fucoxanthin (17–93%), followed by 19′-hexanoyloxyfucoxanthin (3–66%) and 19′-butanoyloxyfucoxanthin

(1.6–27%). Diadinoxanthin (8–100%), alloxanthin (0–85%), diatoxanthin (0–41%), and β-carotene (0–33%) were the photoprotective pigments that mostly contributed to [PPC].

2.3. CHEMTAX Analysis of Pigment Data

The relative abundance of phytoplankton taxonomic groups contributing to monovinyl chlorophyll *a* concentration was estimated from pigment data using CHEMTAX v1.95 chemical software [*Mackey et al*., 1996]. This approach requires as input a matrix with initial diagnostic pigment to chlorophyll *a* concentration ratios that are representative of the region of interest. The initial pigment ratios of the major algal classes were obtained from pigment matrices used in studies from the western Antarctica Peninsula that included microscopy data sets to anticipate the CHEMTAX grouping [*Rodriguez et al*., 2002; *Kozlowski et al*., 2011]. In order to minimize variations in pigment ratios with irradiance and/or nutrient availability along the vertical, data were split into two bins according to sample depth (0–50 and 50–100 m) [*Mendes et al*., 2012]. An output matrix of the diagnostic pigment to chlorophyll *a* concentration is obtained by using a factor analysis and steepest-descent algorithm that points out the best fit of the data to an initial pigment ratio matrix [*Mackey et al*., 1996]. The CHEMTAX procedure used in this work is described in detail by *Mendes et al*. [2012].

Based on previous works in the studied region and the diagnostic pigments detected in our samples, the following algal groups were loaded into the CHEMTAX running: diatoms, dinoflagellates, *Phaeocystis antarctica*, cryptophytes, and green flagellates. We also included peridinin-lacking autotrophic dinoflagellates and diatoms with chlorophyll c_3 as a single chemotaxonomic group, denoted here as dinof$_2$/diato$_2$. This mixed group is characterized by a pigment signature that includes chlorophyll c_3, chlorophyll c_2, 19′-butanoyloxyfucoxanthin, fucoxanthin, and 19′-hexanoyloxyfucoxanthin [*Wright and Jeffrey*, 2006]. Previous surveys evidenced that dinof$_2$/diato$_2$ is an important contributor to the phytoplankton assemblage in the eastern Antarctic Peninsula (as confirmed in this study), with dominances of the dinoflagellate *Gymnodinium* spp. (<20 μm) and the diatom *Pseudo-nitzschia* spp. (<10 μm) [*Mendes et al*., 2012, 2013]. Reasonable agreements have been observed between HPLC-CHEMTAX and microscope-derived biomass of representative taxonomic groups in the Antarctic Peninsula [e.g., *Mendes et al*., 2012].

2.4. Determination of Phytoplankton Absorption Coefficients

A volume of 1–2 L of water was concentrated on GF/F filters and immediately preserved in liquid nitrogen. Absorption of particulate material was determined using the TR method of *Tassan and Ferrari* [1995] using a spectrophotometer (Lambda 35, Perkin Elmer) with an integrating sphere. Optical density (OD, no unit) of samples and blank filters were first measured against air from 390 to 750 nm at the entrance of the sphere and then placed directly against the exit of the sphere, backed with a light trap, for a second scan. Blanks and sample filters were treated with a few drops of 0.5% NaClO for 10–15 min and then carefully washed with 0.2 μm filtered seawater. The extracted filters were measured as described above. Using the correction of pathlength amplification described in *Tassan et al*. [2000], the OD values were converted into absorption coefficients after subtraction of values averaged between 745 and 750 nm (null correction) and correction for the filtered volume and the clearance area of the filter. The spectral absorption coefficients of phytoplankton, $a_{\mathrm{ph}}(\lambda)$ in m^{-1}, were computed as the difference between absorption coefficients before (total particulate) and after (detritus) the NaClO extraction. To examine differences in the shape of phytoplankton absorption spectra, each phytoplankton absorption spectrum was normalized by the average of all values between 400 and 700 nm [*Garver et al*., 1994]. The normalized spectrum is denoted as $a_{<\mathrm{ph}>}(\lambda)$.

2.5. Estimation of the Package Effect From Phytoplankton Absorption Spectra

Ciotti et al. [2002] developed a model that reconstructs the shape of $a_{<\mathrm{ph}>}(\lambda)$ using a linear combination of two spectra representing complementary contributions of the smallest (picophytoplankton) and largest cell sizes (microphytoplankton). We used a least squares Levenberg-Marquardt algorithm to fit each observed $a_{<\mathrm{ph}>}(\lambda)$ spectrum to a linear model by adjusting the values of the derived parameter, S_f [*Ciotti et al*., 2002, equation 3]. This procedure yields an estimate of S_f (no unit) that is consistent with a given observed spectrum of $a_{<\mathrm{ph}>}(\lambda)$ and the model-reconstructed spectrum of $a_{<\mathrm{ph}>}(\lambda)$. The picophytoplankton vector used here was provided by *Ciotti and Bricaud* [2006]. The values of S_f are constrained to vary from 0 to 1. S_f tends to 0 when large cells of phytoplankton (>20 μm) are dominant, and 1 when small cells (<2 μm) dominate. Originally S_f is referred to as the "size factor" [in the sense of *Ciotti et al*., 2002], as most of the variability in the package effect of phytoplankton absorption is controlled by the dominant cell size. With an increase in

accessory pigment concentrations that does not covary with chlorophyll *a* concentration and algal size, the blue-to-red ratio of absorption tends to increase and the absorption spectra become less flat. Thus, S_f is a proxy for combined changes of pigment packaging due to increases of cell size and the concentration of accessory pigments. As the S_f model was established for surface waters, its use to samples collected also in depth (this study) reveal photoacclimation responses to the vertical light variation.

2.6. Cluster Analysis

We performed a cluster analysis for grouping the observed shapes of phytoplankton absorption spectra, $a_{<ph>}(\lambda)$. The *k*-means clustering, implemented in MATLAB (kmeans.m routine), was chosen as an iterative algorithm that assigns objects to clusters so that the sum of distances from each object to its cluster centroid, over all clusters, is minimum. The squared Euclidian distance was used, in a way that each centroid is the mean of the points (i.e., an average $a_{<ph>}(\lambda)$ spectrum) in a cluster. By default, *k*-means begins the clustering process using a randomly selected set of initial centroid locations. The algorithm reassigns points among clusters to decrease the sum of point-to-centroid distances and recomputes cluster centroids for the new cluster assignments. This approach differs from the Hierarchical Cluster Analysis, usually used to group sets of optical spectra [*Lubac and Loisel*, 2007; *Taylor et al*., 2011; *Torrecilla et al*., 2011; *Uitz et al*., 2015], which builds a hierarchical cluster tree. The number of appropriate clusters using the *k*-means method is chosen after inspection of a silhouette diagram, which displays a measure of how close a given sample is to its assigned cluster [*Kaufmann and Rousseeuw*, 1990]. The value in the silhouette diagram ranges from −1 to +1. A high silhouette value indicates that a sample is well matched to its own cluster, and poorly matched to neighboring clusters (see later). If most points have a high silhouette value, then the clustering solution is appropriate. If many samples have a low or negative silhouette value, then the clustering solution may have either too many or too few clusters. The *k*-means method provided groups in which the spectra within a given cluster were less variable than those provided by the Hierarchical Cluster Analysis for our $a_{<ph>}(\lambda)$ data set.

3. Results and Discussion

Three hydrographical conditions were observed at surface during the 2013 surveys: warmer and less salty waters in the Gerlache Strait (GS, −0.11 to 2.15°C; mean of 0.99; and 33.78–34.39; mean of 34.01), intermediate temperature and saltier waters in the Bransfield Strait (BS, −1.52 to 1.86°C; mean of 0.59; and 33.78–34.33; mean of 34.13), and colder and less salty waters in the northwestern Weddell Sea (NWW, −1.26 to 1.12°C; mean of −0.39; and 33.55–34.40; mean of 33.82), revealing the proximity to the ice edge. In 2014, a noteworthy feature was the warmer (–0.54 to 1.32; mean of 0.32) and saltier surface waters (34–34.5; mean of 34.15) in NWW compared to 2013, as the sampling in the Weddell Sea was not close to the ice edge as in the previous year. This was also revealed by very deeper mixed layer depths, defined as the depth where occurs a change of density of 0.05 kg m^{-3} relative to the surface, Z_{MLD} (98 m) compared to 2013 (55 m) in NWW. The average Z_{MLD} was 29 m (2013) and 71 m (2014) in BS and 71 m (2013) and 55 m (2014) in GS. The Z_{MLD} was shallower than Z_{eu} at most of the stations (Table 1), revealing vertically stratified waters [*Uitz et al*., 2006]. Figure 2 shows a typical profile in BS (2013) of temperature, salinity, and pigment ratios of phytoplankton, with Z_{eu} and Z_{MLD} also shown. A increase of [PSC]/[TChl *a*] followed by a decrease of [PPC]/[TChl *a*] along depth indicates that phytoplankton is close to being light-limited below Z_{MLD} (Figure 2).

The ranges of [TChl *a*] were similar in 2013 (0.10–3.03 mg m^{-3}) and 2014 (0.12–2.99 mg m^{-3}), however with differences among regions (Table 1). The main contributors to the phytoplankton biomass, as estimated by CHEMTAX, were diatoms, dinof$_2$/diato$_2$ and cryptophytes, although in 2013 *P. antarctica* made an important contribution in GS (18–45% in $L_{>37\%}$). A detailed description of the phytoplankton composition observed in GS is found in *Mendes et al*. [2017]. In BS, the proportion of diatoms was low to moderate in 2013 (13–58% in $L_{<37\%}$), but contributed substantially to the phytoplankton biomass in all regions in 2014 (0–81% in $L_{>37\%}$). In 2013, dinof$_2$/diato$_2$ was dominant in NWW (up to 77% in $L_{>37\%}$), with contributions of about two-to-threefold larger in 2014 in both GS and BS and reaching 83% in $L_{<10\%}$ in GS. The presence of cryptophytes was always important (Table 1), excepted in BS during 2013 (mean of 9% in $L_{>37\%}$) and in NWW during 2014 (mean of 8% in $L_{>37\%}$). In the two stations sampled in NWW$_{HT}$ in 2014, CHEMTAX revealed diatom-dominated assemblages, with contributions up to 77% in $L_{>37\%}$. As will be next seen from their absorption spectra, it is very unlikely that those samples contained a high proportion of diatoms.

Table 1. The Range and Mean Values of the Ratio of Z_{eu}/Z_{MLD}, Total Chlorophyll *a* Concentration and the Percentage of Contribution of the Main Taxonomic Groups of Phytoplankton Estimated by CHEMTAX

Region	Z_{eu}/Z_{MLD}	Depth	[TChl *a*] (mg m^{-3})	Diatom (%)	dinof$_2$/diato$_2$ (%)	Cryptophyte (%)	*P. antarctica* (%)	*N*
2013								
GS	0.8–8 (3.1)	$L_{>37\%}$	0.71–1.47 (1.09)	13–58 (30)	4–13 (7)	7–52 (30)	18–45 (35)	9
		$L_{37-10\%}$	0.80–1.27 (1.11)	7–58 (29)	2–11 (6)	7–77 (33)	13–46 (31)	6
		$L_{<10\%}$	0.20–1.26 (0.46)	16–56 (39)	3–37 (17)	0–46 (9)	20–48 (28)	9
BS	0.2–6.3 (1.3)	$L_{>37\%}$	0.36–3.03 (1.27)	18–86 (59)	1–41 (12)	0–29 (9)	6–35 (16)	44
		$L_{37-10\%}$	0.47–2.23 (1.48)	5–86 (54)	1–40 (15)	0–29 (11)	9–33 (18)	16
		$L_{<10\%}$	0.15–2.65 (0.96)	16–89 (60)	2–46 (15)	0–22 (6)	5–31 (15)	34
NWW	0.4–4.1 (1.5)	$L_{>37\%}$	0.71–2.25 (1.23)	3–24 (9)	16–77 (41)	0–65 (36)	0–8 (5)	31
		$L_{37-10\%}$	0.35–0.80 (1.12)	3–22 (10)	23–78 (46)	0–62 (28)	0–8 (5)	28
		$L_{<10\%}$	0.10–1.76 (0.61)	1–39 (18)	21–85 (56)	1–71 (15)	0–11 (5)	66
2014								
GS	0.9–15.5 (4.8)	$L_{>37\%}$	0.99–2.20 (1.66)	20–48 (35)	4–31 (14)	24–66 (45)	1–8 (4)	14
		$L_{37-10\%}$	0.41–1.68 (1.18)	29–51 (36)	9–44 (26)	2–56 (30)	2–9 (5)	7
		$L_{<10\%}$	0.16–2.67 (0.88)	1–57 (39)	3–83 (28)	2–70 (24)	2–13 (7)	12
BS	0.4–7.5 (1.8)	$L_{>37\%}$	0.29–2.99 (1.37)	0–81 (21)	5–69 (32)	0–94 (38)	0–14 (5)	36
		$L_{37-10\%}$	0.40–2.87 (1.24)	0–80 (32)	8–64 (31)	2–90 (28)	2–11 (6)	20
		$L_{<10\%}$	0.14–2.27 (0.63)	0–79 (41)	9–62 (28)	3–87 (20)	1–20 (7)	47
NWW	0.4–4.2 (0.9)	$L_{>37\%}$	0.31–1.67 (0.74)	4–36 (19)	47–76 (61)	0–24 (8)	0–9 (3)	15
		$L_{37-10\%}$	0.44–1.62 (0.98)	7–52 (26)	36–67 (53)	0–26 (13)	0–10 (3)	13
		$L_{<10\%}$	0.15–0.71 (0.74)	20–61 (43)	17–64 (33)	3–27 (11)	0–22 (6)	35
NWW$_{HT}$	1.6–2.9[a]	$L_{>37\%}$	0.12–0.16 (0.13)	72–77 (75)	1–3 (2)	0	19–22 (20)	4
		$L_{37-10\%}$	0.13–0.16 (0.14)	61–62 (62)	7–7 (7)	3–7 (5)	20–25 (23)	2
		$L_{<10\%}$	0.14–0.24 (0.18)	8–20 (13)	42–58 (48)	1–3 (2)	15–25 (19)	6

[a]The mean of Z_{eu}/Z_{MLD} is not shown as values in NWW$_{HT}$ correspond to two stations.

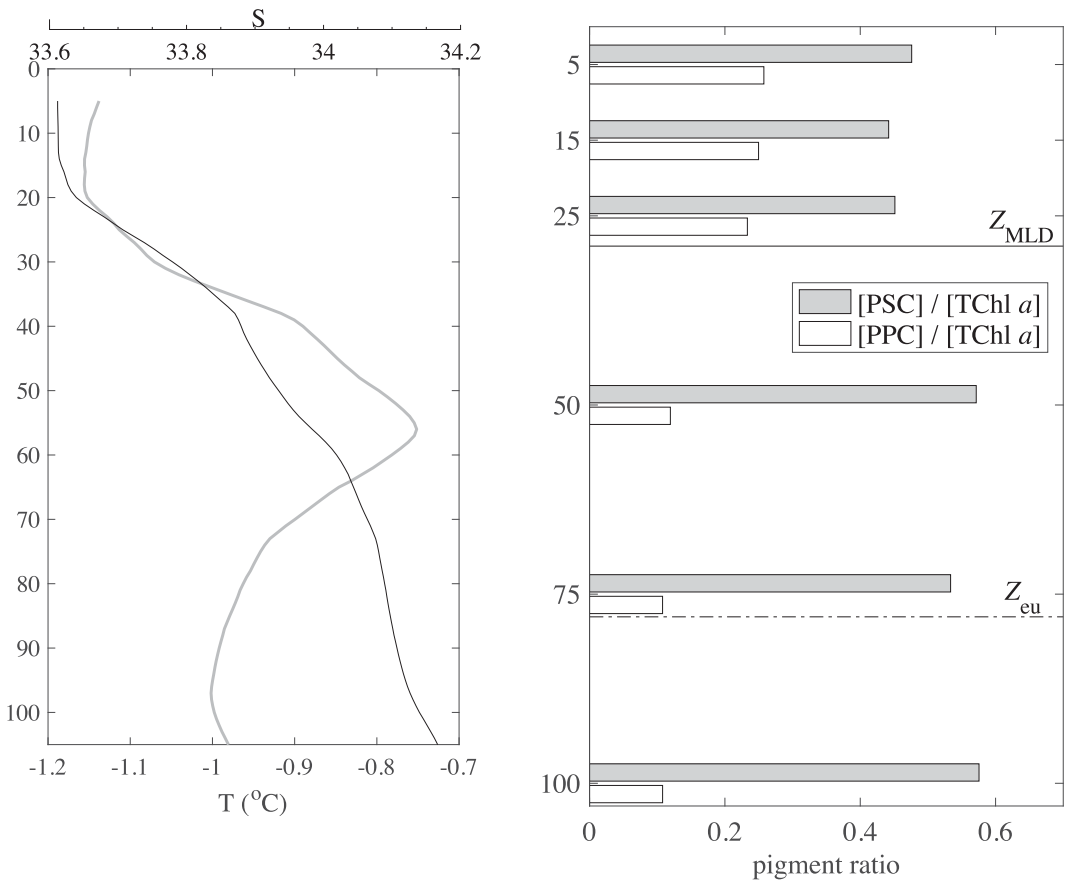

Figure 2. Example of typical vertical profiles of (left) temperature (thick grey line, T°C) and salinity (thin black line, S) and (right) [PSC]/[TChl *a*] and [PPC]/[TChl *a*] observed in the Bransfield Strait in 2013. The mixed layer depth (Z_{MLD}) and the euphotic depth (Z_{eu}) are also shown.

These discrepancies are probably related to very different pigment composition compared to the main domain of our sampling, that is, close to the coast and the ice edge near the tip of Antarctic Peninsula (Figure 1). Previous studies characterized the distribution and composition of phytoplankton assemblages in relation to environmental conditions in GS [*Rodriguez et al.*, 2002; *Varela et al.*, 2002; *Mendes et al.*, 2017], BS [*Rodriguez et al.*, 2002; *Varela et al.*, 2002; *Mendes et al.*, 2012, 2013; *García-Muñoz et al.*, 2013; *Gonçalves-Araújo et al.*, 2015], and NWW [*Kang et al.*, 2001; *García-Muñoz et al.*, 2013]. These studies observed that the water column stability is one of the most important factors determining the distribution of biomass and taxonomic composition of phytoplankton around the Antarctic Peninsula.

3.1. Variability in the Specific Absorption Coefficients of Phytoplankton

The absorption coefficients of phytoplankton at 440 and 676 nm, $a_{ph}(440)$ and $a_{ph}(676)$, varied broadly, from about 0.006 to 0.135 and 0.002 to 0.064 m^{-1}, respectively, accompanying the large variability in [TChl *a*] (Figure 3). The chl *a*-specific absorption coefficient of phytoplankton at 440 nm, $a^*_{ph}(440)$, ranged from about 0.020 to 0.102, 0.015 to 0.094, and 0.022 to 0.086 m^2 (mg chl *a*)$^{-1}$ in $L_{>37\%}$, $L_{37-10\%}$, and $L_{<10\%}$, respectively, with averages virtually identical (0.043, 0.044, and 0.044 m^2 (mg chl *a*)$^{-1}$). The chl *a*-specific absorption coefficient of phytoplankton at 676 nm, $a^*_{ph}(676)$, varied less than $a^*_{ph}(440)$, from 0.010 to 0.045, 0.007 to 0.045, and 0.012 to 0.034 m^2 (mg chl *a*)$^{-1}$ for $L_{>37\%}$, $L_{37-10\%}$, and $L_{<10\%}$, respectively (identical average of 0.021 m^2mg chl *a*)$^{-1}$ for each of 3 layers). Values of $a^*_{ph}(676)$ are noticeably higher compared to what is generally reported in literature and this is probably associated with very small cell size of phytoplankton, low pigment concentration per cell and also the presence of chlorophyll *b*.

Values of $a^*_{ph}(440)$ and $a^*_{ph}(676)$ did not differ statistically among depths (ANOVA and multiple comparison test). Therefore, an empirical relationship between $a_{ph}(440)$ and $a_{ph}(676)$ and [TChl *a*] was determined on the basis of all data in the form of a power law (Figure 3). Figure 3 also shows the power law relationship obtained by *Bricaud et al.* [1995] (B95) based on different regions of the world ocean, not including the Southern Ocean. Despite some deviation of our data to the extremes of B95's line, our values of $a_{ph}(440)$ and $a_{ph}(676)$ seem to be reasonably well represented by B95 and are within the dispersion of the global data, i.e., a factor of 4 for a given [TChl *a*].

The proportion of [PSC] relative to [TChl *a*] showed an inverse pattern with respect to [TChl *a*] considering all depths (Figure 4a). [PSC]/[TChl *a*] varied mostly between 0.1 and 0.7 in $L_{>37\%}$ and $L_{37-10\%}$. Higher [PSC]/[TChl *a*] (between 0.5 and 1) were found in $L_{<10\%}$, albeit several $L_{<10\%}$ samples exhibited [PSC]/[TChl *a*] in the same range as $L_{>37\%}$ and $L_{37-10\%}$. Much greater [PSC]/[TChl *a*] (~0.75) associated with low [TChl *a*] (~0.15 mg m^{-3}) in $L_{>37\%}$ and $L_{37-10\%}$ corresponded to samples in NWW_{HT}. Figure 4a shows both site-to-site

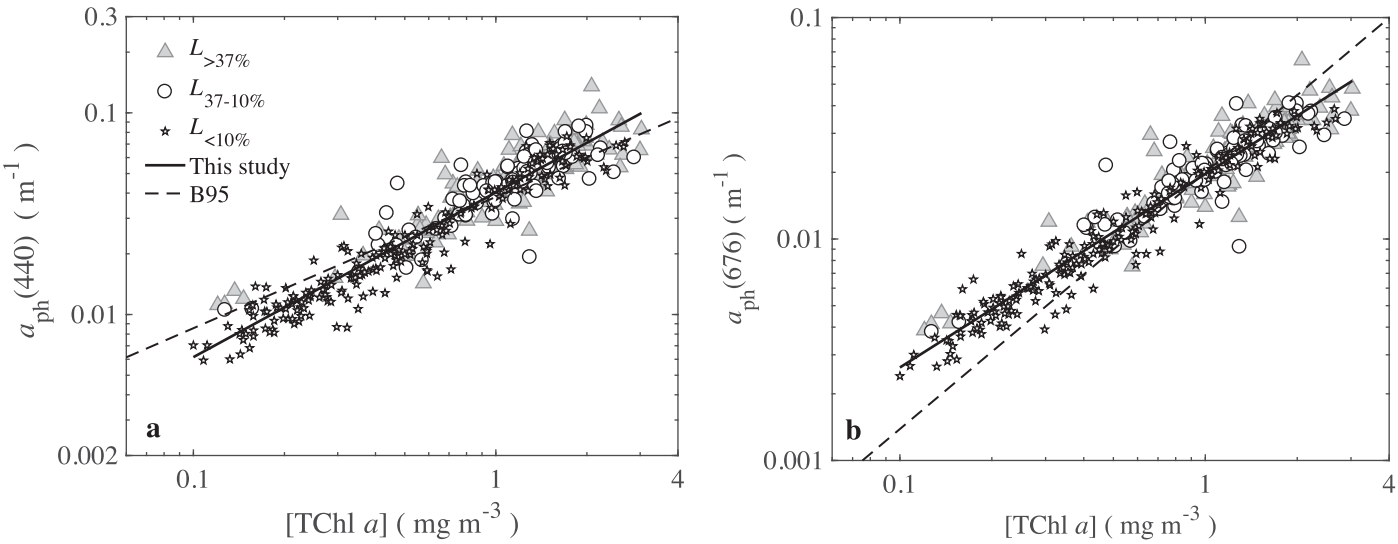

Figure 3. The phytoplankton absorption coefficient, $a_{ph}(\lambda)$, at (a) 440 nm and (b) 676 nm, as a function of total chlorophyll *a* concentration, [TChl *a*], in $L_{>37\%}$, $L_{37-10\%}$, and $L_{<10\%}$.The regression formula and the best fit parameters for this study are $a_{ph}(440) = 0.042$ [TChl *a*]$^{0.739}$ ($R^2 = 0.90$; $p < 0.00001$; $N = 455$) and $a_{ph}(676) = 0.020$ [TChl *a*]$^{0.794}$ ($R^2 = 0.93$; $p < 0.00001$; $N = 455$), shown as continuous lines. The dashed line represents the best fit regressions observed by *Bricaud et al.* [1995] (B95).

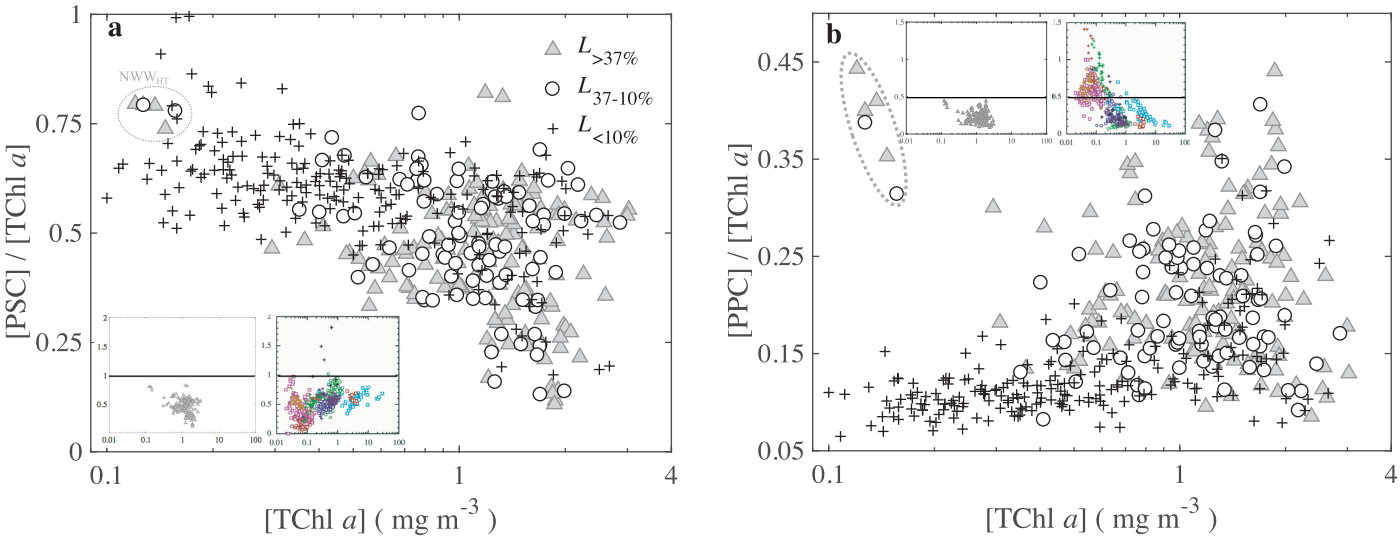

Figure 4. The sum of (a) photosynthetic, [PSC], and (b) photoprotective, [PPC], pigments to total chlorophyll *a* concentration, [TChl *a*], as a function of [TChl *a*]. The circles identify $L_{>37\%}$ and $L_{37-10\%}$ samples in NWW$_{HT}$ (excluding the stars within the circle in Figure 4a). The inset graphs compare the ranges of [PSC]/[TChl *a*] and [PPC]/[TChl *a*] in $L_{>37\%}$ to those observed by Bricaud *et al.* [2004] (only within the first optical depth, denoted as $L_{>37\%}$ here) for various regions worldwide (their Figure 3). Note the same scale in and *y* axes as in *Bricaud et al.* [2004] for the inset figures. The dashed lines are references for visual comparison. The different symbols in *Bricaud et al.* inset graphs discriminate cruises. For details, see *Bricaud et al.* [2004].

and vertical variations of [PSC]/[TChl *a*], with a general decrease with [TChl *a*], because greater [PSC] is associated with lower [TChl *a*] in depth (Figure 2). Values of [PSC]/[TChl *a*] did not differ between $L_{>37\%}$ and $L_{37-10\%}$, but was significantly higher in $L_{<10\%}$ (ANOVA and multiple comparison test, $p < 0.0001$). In contrast to [PSC]/[TChl *a*], [PPC]/[TChl *a*] showed an increasing pattern with [TChl *a*], mainly driven by low [PPC]/[TChl *a*] found in $L_{<10\%}$ (mostly between 0.06 and 0.2, Figure 4b). As for [PSC]/[TChl *a*], [PPC]/[TChl *a*] was relatively much higher in NWW$_{HT}$, varying from 0.35 to 0.44. [PPC]/[TChl *a*] was significantly higher in $L_{>37\%}$ comparing to $L_{37-10\%}$ and lower in $L_{<10\%}$ (ANOVA and multiple comparison test, $p < 0.0001$), in agreement to a continuously [PPC] decreasing from the surface to deeper waters [*Bricaud et al.*, 1995; *Trees et al.*, 2000].

A comparison with the ranges of photosynthetic and photoprotective pigments relative to [TChl *a*] found by *Bricaud et al.* [2004] regarding various regions from the world's oceans (only for $L_{37\%}$ and not including Antarctic waters) shows that both [PSC]/[TChl *a*] and [PPC]/[TChl *a*] in our study (inset graphs in Figure 4) are within the ranges found for mesotrophic and eutrophic waters in subtropical and temperate latitudes. The [PSC]/[TChl *a*] and [PPC]/[TChl *a*] values observed here are also in agreement with ranges observed for various oceanographic provinces [*Sathyendranath et al.*, 2005]. This is an important aspect as it does not agree with the expectation of greater proportions of photosynthetic pigments in phytoplankton assemblages to increase light harvesting due to relatively low irradiance available in polar areas. Note that the samples were taken during middle/late summer, thus, they do not represent average growth conditions, which can only be described when similar analyses and comparisons are performed in other periods for the studied area. Similar proportions of photoprotective pigments to those for lower latitudes suggest that algal communities around the Antarctic Peninsula are not light limited in summer [see also *Mendes et al.*, 2012, 2017]. In fact, during our surveys, the ratios of Z_{eu} to Z_{MLD} were generally higher than 1, which implies that phytoplankton cells within Z_{MLD} probably did not experience light limitation while they mixed vertically through the mixed layer. Combined effects of the dominant cell size of phytoplankton and [PSC]/[TChl *a*] and [PPC]/[TChl *a*] ranges observed here resulted in $a^*_{ph}(\lambda)$ values similar to other regions worldwide (Figure 3).

The effect of accessory pigments in $a^*_{ph}(\lambda)$ variations were investigated through the ratios [PSC]/[PSC + PPC] and [PPC]/[PSC + PPC]. Values of $a^*_{ph}(440)$ were not correlated to [PSC]/[PSC + PPC] or [PPC]/[PSC + PPC] at any depth, but the highest [PSC]/[PSC + PPC] observed in NWW$_{HT}$ (Figure 1) were associated with very high $a^*_{ph}(440)$ values (>0.085 m^2 (mg Chl *a*)$^{-1}$). Very high $a^*_{ph}(440)$ however, likely results from the combination of larger concentrations of accessory pigments and small cell size of *Phaeocystis* spp. (see Cluster 1 in section 3.4). The scatter in the $a^*_{ph}(440)$ versus [TChl *a*] (Appendix B), [PSC]/[PSC + PPC] and [PPC]/[PSC + PPC] (Figure 5) relationships reveals that variations in $a^*_{ph}(\lambda)$ did not clearly follow changes in

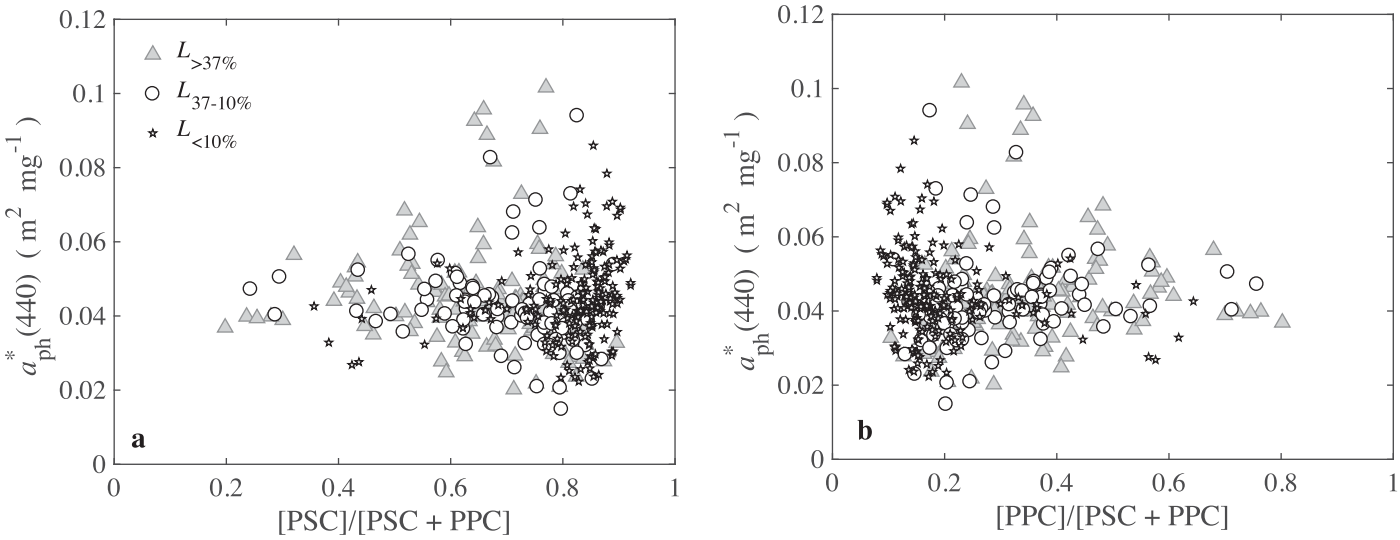

Figure 5. The chlorophyll-specific absorption coefficient of phytoplankton at 440 nm, $a^*_{ph}(440)$ as a function of the ratios (a) [PSC]/[PSC + PPC] and (b) [PPC]/[PSC + PPC].

chlorophyll *a* [see also *Segura et al.*, 2013] nor the proportions of photosynthetic or photoprotective carotenoids. The coefficient $a^*_{ph}(\lambda)$ is generally found to vary inversely to chlorophyll *a* concentration, as a result of an increasing package effect with chlorophyll *a* and an inverse covariation between the relative abundance of accessory pigments to chlorophyll *a*, although with a large scatter [*Bricaud et al.*, 1995]. It noteworthy that no clear pattern was found between [TChl *a*] and dominant cell size for which samples chlorophyll *a* size fractionation was available (Appendix A). For instance, relatively high [TChl *a*] of 1.83 and 2.49 mg m^{-3} were associated with percentages of picophytoplankton of 62% and 60%, respectively. This may partially explain the lack of a clear inverse pattern of $a^*_{ph}(\lambda)$ and [TChl *a*].

While the $a^*_{ph}(\lambda)$ spectra will be flattened due to increase of cell size of phytoplankton [*Duysens*, 1956], the covariation of $a^*_{ph}(440)$ and $a^*_{ph}(676)$ ($r = 0.95$, $p < 0.00001$, $N = 455$) implies that accessory pigments absorbing at these wavelengths are covarying with chlorophyll *a*. The total concentration of accessory pigments is highly correlated to [TChl *a*] ($r = 0.96$, $p < 0.00001$, $N = 455$) [see also *Trees et al.*, 2000]. Therefore, the combined effect of [TChl *a*] and accessory pigments could not be separated in this data set, except in the case of a very high proportion of photosynthetic pigments (Figure 5a), resulting in high values for $a^*_{ph}(440)$ (>0.085 m^2 (mg Chl *a*)$^{-1}$), but not for $a^*_{ph}(676)$ (Appendix B).

An increasing chlorophyll *a* content per cell is expected from the surface to deeper waters as a result of photoacclimation, revealing a decrease in $a^*_{ph}(\lambda)$ along the vertical. A reduction in $a^*_{ph}(\lambda)$ in depth was not observed here. One possible explanation should be a regular increasing [PSC]/[TChl *a*] along depth, rather than an increasing chlorophyll content per cell, resulting in identical averages of $a^*_{ph}(\lambda)$ in $L_{>37\%}$, $L_{37-10\%}$, and $L_{<10\%}$ (Figure 3), but also vertical variations in the dominant cell size of phytoplankton. In principle, an increasing proportion of [PPC] relative to chlorophyll *a* favors an increase in $a^*_{ph}(\lambda)$ in the blue part of the spectrum. Because both [PPC] and [TChl *a*] are higher in the upper layers (and lower in depth), greater [PPC] should not necessarily result in higher $a^*_{ph}(440)$ near surface than in depth. Note that the wide dispersion of [PSC]/[TChl *a*] and [PPC]/[TChl *a*] within the sampled layers, especially for $L_{>37\%}$ (Figure 4), may be caused by changes in the "average light" to which the phytoplankton cells were exposed among stations, and also in phytoplankton community composition.

The interpretation of the effect of changes in [TChl *a*] and accessory pigments in $a^*_{ph}(\lambda)$ is not straightforward mainly because [TChl *a*] and accessory pigments strongly covary. Lower and higher [TChl *a*] (over a range of 0.10–3.03 mg m^{-3}) do not necessarily result in higher and lower $a^*_{ph}(\lambda)$, respectively, in Antarctic waters. Similarly, lower and higher [PSC]/[PSC + PPC] or [PPC]/[PSC + PPC] are not associated with lower and higher $a^*_{ph}(440)$ or at any in the blue spectral region. While it is acknowledged that $a^*_{ph}(\lambda)$ vary in a regular manner with chlorophyll *a* concentration [*Bricaud et al.*, 1995], regular variations of $a^*_{ph}(\lambda)$, even along the vertical, are not necessarily observed in our data set. This is an important aspect as most of the

studies on phytoplankton absorption in Antarctica to date discuss the pigment packaging and influence of accessory pigments to spectral phytoplankton absorption in terms of $a^*_{ph}(\lambda)$ [e.g., *Mitchell and Holm-Hansen*, 1991; *Sosik et al.*, 1992; *Arrigo et al.*, 1998; *Reynolds et al.*, 2001].

3.2. Absorption Ratios as Related to Accessory Pigments

The ratio [PSC]/[TChl *a*] explained about 69% of the variation in $a_{ph}(440)/a_{ph}(490)$ in all depths (Figure 6a). [PPC]/[TChl *a*] increased regularly with $a_{ph}(460)/a_{ph}(490)$, consistently with a major influence of photoprotective pigments at 460 nm (Figure 6b). The values of [PPC]/[TChl *a*] in $L_{<10\%}$ followed the same average trend observed for $L_{>37\%}$ and $L_{37-10\%}$. This result suggests that phytoplankton assemblages at low irradiance ($L_{<10\%}$) contain enough [PPC] relative to [TChl *a*] to cause an increase in $a_{ph}(460)/a_{ph}(490)$ (the initial part of the regression line in Figure 6b). In fact, many $L_{<10\%}$ samples show [PPC]/[TChl *a*] in the same range observed in $L_{>37\%}$ and $L_{37-10\%}$. This reflects different rates of mixing of phytoplankton cells in the water column and photoacclimation, which in turn depends on whether the lower light depths lie below or within the mixed layer. A dependence of $a_{ph}(440)/a_{ph}(676)$ and [PPC]/[TChl *a*] was also found ($a_{ph}(440)/a_{ph}(676) = 1.97 + 0.69$[PPC]/[TChl *a*]; $R^2 = 0.40$; $p < 0.00001$; $N = 455$).

Our results support the notion that the absorption ratios of $a_{ph}(440)/a_{ph}(490)$ and $a_{ph}(460)/a_{ph}(490)$ are useful to predict [PSC]/[TChl *a*] and [PPC]/[TChl *a*], and vice versa, if both information are not concomitantly available. The utility of these wavelengths to derive information on carotenoids to chlorophyll *a* ratios in other regions of Antarctica should be further investigated. This aspect is relevant for satellite observations of ocean color and has been suggested previously [*Sathyendranath et al.*, 2005]. The inclusion of the 460 nm band in ocean color satellite sensors is noteworthy as many pigments are stronger absorbers of light around this wavelength [*Hoepffner and Sathyendranath*, 1991].

3.3. Proxy of Package Effect of Phytoplankton

Because the effects of biomass, cell size, and accessory pigments of phytoplankton on $a^*_{ph}(\lambda)$ are intermingled, we use the parameter S_f, estimated independently of chlorophyll *a* (in contrast to $a^*_{ph}(\lambda)$) to investigate variations in spectral shape of phytoplankton absorption and the sources of this variability.

A typical negative covariation between S_f and chlorophyll *a* concentration is observed [e.g., *Bricaud et al.*, 2012] because an increase in the phytoplankton chlorophyll biomass is generally accompanied by an increase in the dominant cell size, consistent with an increasing package effect (low S_f). However, this may not hold in depth, where photoacclimation due to lower irradiance may induce changes in the spectral shape of $a_{ph}(\lambda)$ relatively to the surface, independently of changes in phytoplankton cell size. Indeed, most

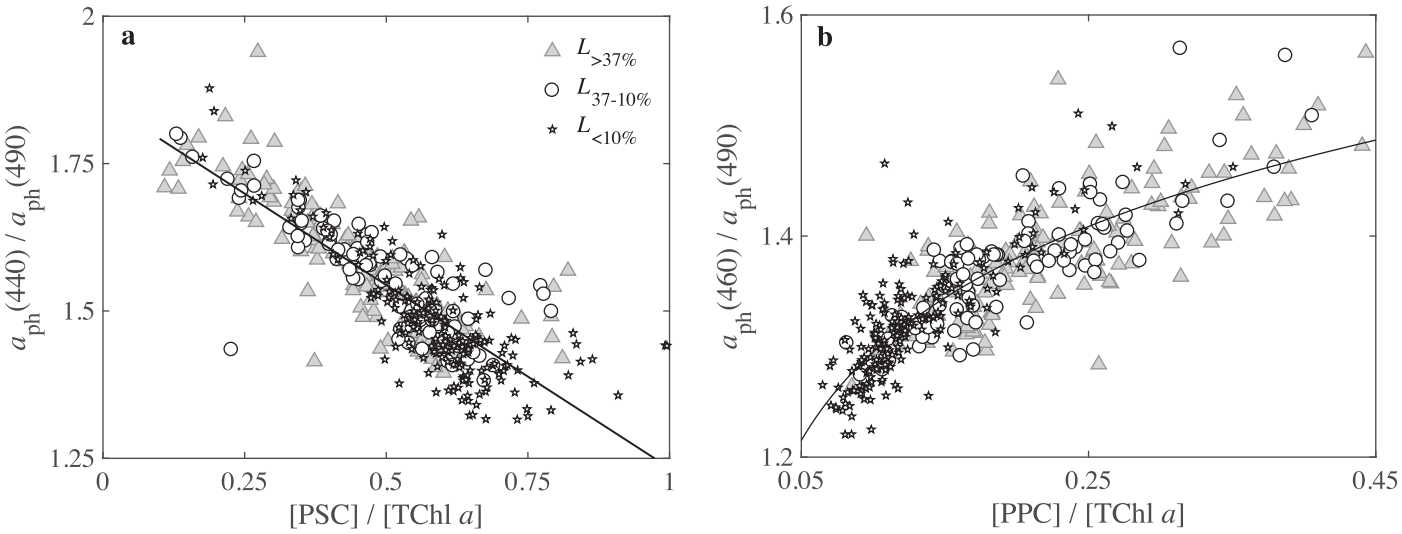

Figure 6. (a) The absorption ratio $a_{ph}(440)/a_{ph}(490)$ as a function of the proportion of photosynthetic pigments to total chlorophyll *a* concentration, [PSC]/[TChl *a*]. (b) The absorption ratio $a_{ph}(460)/a_{ph}(490)$ as a function of the proportion of photoprotective pigments to [TChl *a*], [PPC]/[TChl *a*]. The regression formula and the best fit parameters for this study are $a_{ph}(440)/a_{ph}(490) = 1.85 - 0.62$[PSC]/[TChl *a*] ($R^2 = 0.69$; $p < 0.00001$; $N = 455$) and $a_{ph}(460)/a_{ph}(490) = 3.44$[PPC]/[TChl *a*]$^{0.67}$ ($R^2 = 0.72$ for log-transformed data; $p < 0.00001$; $N = 455$), shown as continuous lines.

of the $L_{<10\%}$ data depart from the average trend based on $L_{>37\%}$ and $L_{37-10\%}$ data, with lower S_f for a given [TChl *a*], mostly between 0.1 and 0.3 (Figure 7a). Another observation is that S_f is relatively constant (around 0.35) while [TChl *a*] varies more than a factor of 2 (~0.5–2 mg m^{-3}). Consistently with a greater package effect for larger cell size, the lowest S_f (0.16 and 0.24) for samples with information of cell size available (Appendix A) was associated with the highest microphytoplankon contributions (34 and 54%, respectively, Figure A1).

A regular decrease in S_f with an increase of [Fuco]/[TChl *a*] is observed, with S_f values in $L_{<10\%}$ following the same pattern as in $L_{>37\%}$ and $L_{37-10\%}$ (Figure 7b). This implies that an increasing [Fuco] relative to [TChl *a*] is responsible for a greater package effect in depth. S_f covaried less markedly with [PSC]/[TChl *a*] than [Fuco]/[TChl *a*], in which [Fuco] is included. Therefore, fucoxanthin (the diagnostic pigments of diatoms), is confirmed to be the main component of [PSC]/[TChl *a*] responsible for flattening the $a_{ph}(\lambda)$ spectra (lower S_f). The production of fucoxanthin is an important mechanism for diatom assemblages to increase light harvesting in the tip of Antarctic Peninsula as addressed by *Mendes et al*. [2017] and similarly observed in surface Argentinean waters [*Lutz et al*., 2016]. In fact, the production of photosynthetic pigments is feasible in nonlimiting nutrient conditions. The availability of macronutrients during our surveys was always high, with mean concentrations of nitrate, phosphate and silicate of 26.59, 1.86, and 38.28 μM, respectively, in the whole water column (R. Pollery, personal communication, 2014). Also, the phytoplankton communities in the same waters were not limited by iron [*Russo et al*., 2015]. It is noteworthy that the assumption that high [Fuco]/[TChl *a*] is related to a large package effect does not always hold. The two farthest stations in NWW_{HT} were characterized by small phytoplankton cells (*P. antarctica*) (section 3.4), with very high [Fuco]/[TChl *a*] and the weakest package effect ($S_f > 0.5$, Figure 7b).

The [PPC]/[TChl *a*] ratio showed less dispersion with S_f (Figure 7d). The presence of photoprotective pigments, with a primary peak of absorption at ~460 nm and secondary peak at ~490 m, enhances the phytoplankton absorption in the blue spectrum domain, reducing the package effect (higher S_f). Also, there is also the underlying effect of cell size of phytoplankton, as [PPC]/[TChl *a*] is, in general, negatively correlated to size. The xanthophyll cycle of algae is a short-time scale mechanism that comprises the enzymatic conversion of carotenoids such as diadinoxanthin to diatoxanthin in diatoms and haptophytes [*Van Leeuwe et al*., 2005]. In our samples, both pigments made considerable contribution to [PPC], in addition to alloxanthin [see *Mendes et al*., 2017], an important photoprotector in cryptophytes, and β-carotene, that is a photoprotective pigment present in most of the algal groups [*Jeffrey et al*., 1997]. Phytoplankton acclimation in high irradiance occurs at least until 25 m (generally within the mixed depth) in these waters, as suggested by similar [PPC]/[TChl *a*] at 5, 15–25 m. The presence of photoprotective pigments indicates that the algal assemblages in the northern tip of Antarctic Peninsula are adapted to high irradiance [*Mendes et al*., 2017], in agreement with recent works that have shown photoprotective mechanisms of phytoplankton in the Southern Ocean.

The scatter in S_f versus $a^*_{ph}(440)$ is large (Figure 7e) and very similar to that observed for S_f versus $a^*_{ph}(676)$ (not shown), because both coefficients were highly correlated (section 3.1). The lack of coherence of $a^*_{ph}(\lambda)$ and S_f agrees with the expectation that $a^*_{ph}(\lambda)$ at specific wavelengths is not a good indicative of package effect for our data set (section 3.1). In other words, lower and higher values $a^*_{ph}(\lambda)$ were not necessarily associated with lower and higher S_f, respectively.

We conclude that the package effect in the northern Antarctic Peninsula mainly results from an increase in [Fuco] content per cell at depth, although an increase in cell size may also be important. The relative contributions of pigment composition and cell size of phytoplankton to the package effect are, however, intermingled and cannot be distinguished using our data set. The inverse pattern between S_f and [PPC]/[TChl *a*] is a consequence of lower [PPC]/[TChl *a*] in association to higher [Fuco]/[TChl *a*], the inverse covariation of [PPC]/[TChl *a*] and cell size, but also the direct contribution of photoprotective pigments to enhance absorption in the blue part of the spectrum, reducing the package effect. The less marked dispersion between S_f and [PPC]/[TChl *a*] may be indicative of the direct role of photoprotective pigments to control S_f to some extent.

3.4. Cluster Analysis on the Phytoplankton Absorption Spectra

We next examine the variability in the $a_{<ph>}(\lambda)$ spectra through a clustering based on variations in their shape. The silhouette diagram obtained from the partitioning of the $a_{<ph>}(\lambda)$ spectra through the *k*-means

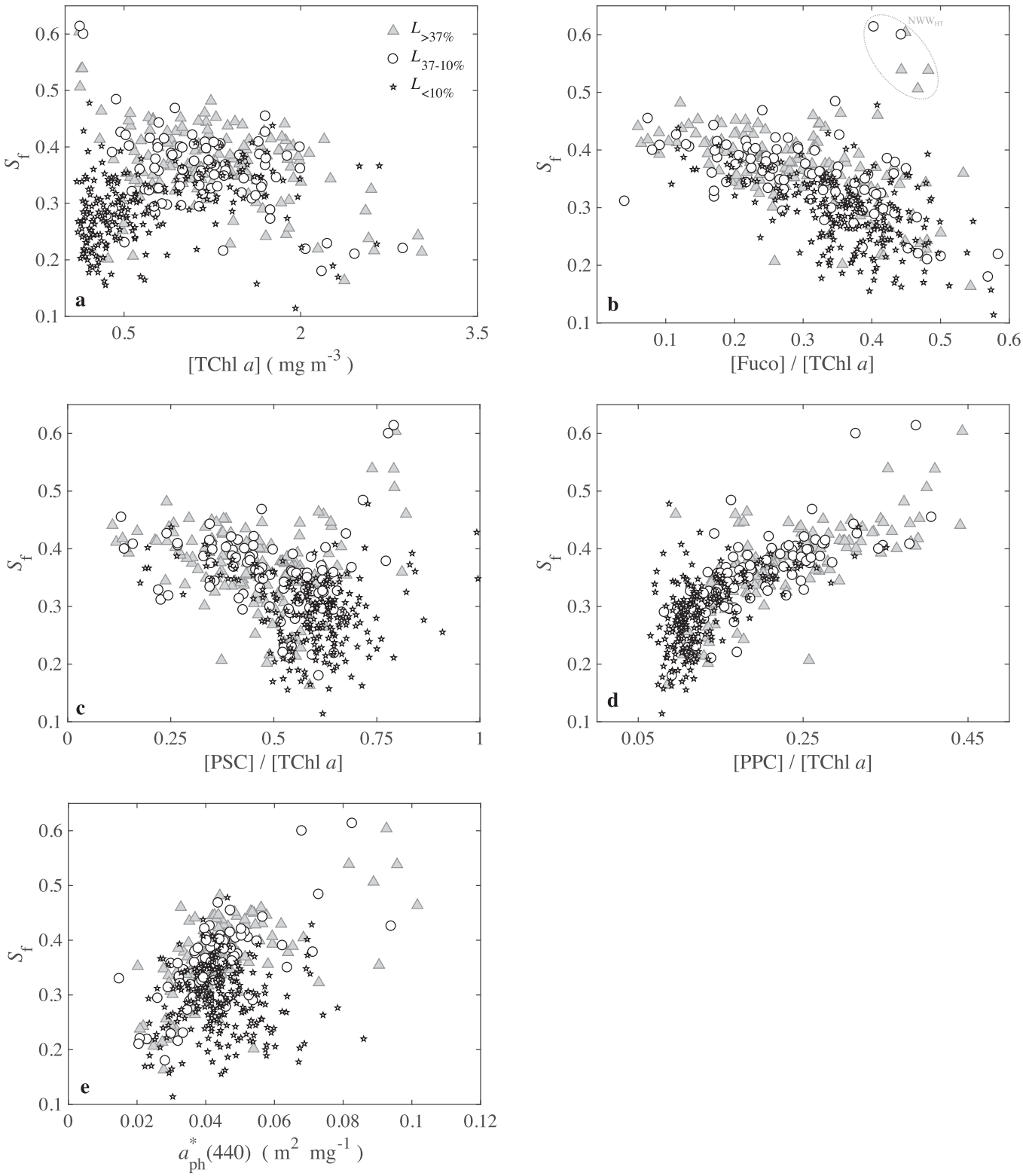

Figure 7. The proxy of package effect, S_f, as a function of (a) total chlorophyll *a* concentration, [TChl *a*], the ratios of concentration of (b) fucoxanthin, [Fuco], (c) photosynthetic pigments, [PSC], (d) photoprotective pigments, [PPC], to [TChl *a*] and (e) the chl *a*-specific absorption coefficient of phytoplankton at 440 nm, $a^*_{ph}(440)$. The ratios of *x* axis values to *y* axis values were not were statistically different (ANOVA and multiple comparison test) in $L_{>37\%}$ and $L_{37-10\%}$. The correlation coefficients are (a) $r = -0.39$, $p = 0.0012$, $N = 244$ in $L_{>37\%}$ and $L_{37-10\%}$; $r = 0.24$, $p < 0.00001$, $N = 208$ in $L_{<10\%}$. (b) $r = -0.45$, $p < 0.00001$, $N = 244$ in $L_{>37\%}$ and $L_{37-10\%}$; $r = -0.52$, $p = 0.055$, $N = 208$ in $L_{<10\%}$; (c) $r = -0.12$, $p = 0.0012$, $N = 244$ in $L_{>37\%}$ and $L_{37-10\%}$; $r = -0.24$, $p < 0.00001$, $N = 208$ in $L_{<10\%}$; (d) $r = 0.72$, $p = 0.0012$, $N = 244$ in $L_{>37\%}$ and $L_{37-10\%}$; $r = 0.56$, $p < 0.00001$, $N = 208$ in $L_{<10\%}$; (e) $r = 0.62$, $p = 0.0012$, $N = 244$ in $L_{>37\%}$ and $L_{37-10\%}$; the correlation was not significant in $L_{<10\%}$.

algorithm shows that seven was the most appropriate number to partition this data set. This means that a minimum number of negative values and a maximum of silhouette values closer to 1 were obtained with seven clusters (Figure 8a). Few $a_{<ph>}(\lambda)$ spectra showed negative silhouette values, indicative of poor classification. These spectra were kept in our analysis as the poor classification seems to be due to a larger variability among spectra of Clusters 3 and 6 from 400 to 420 nm, which does not alter the interpretation of our results. Figures 8b–8h display the $a_{<ph>}(\lambda)$ spectra for each of the seven clusters, showing a very reasonable partitioning according to their shape. The two basis vectors representing the extrema in spectral absorption shapes of phytoplankton used in the S_f model (section 2.5) are shown for comparison. The variability of selected variables within each cluster is presented in Table 2.

In accordance with a gradual spectral flatness from Clusters 1 to 7, the cluster analysis partitioned the $a_{<ph>}(\lambda)$ spectra into different ranges of S_f, with average values of 0.56, 0.41, 0.37, 0.34, 0.30, 0.23, and 0.22, respectively, as revealed by an increasing resemblance of the $a_{<ph>}(\lambda)$ spectra to the microphytoplankton basis vector (Figure 8). Also, the variability of S_f within each cluster was always small, with the lowest CV values (7.8, 5.7, 9.1, 6.8, 7.3, 15.9, and 14.9% from Clusters 1 to 7), compared to those for other variables (Table 2).

As expected from their very different shapes, with the highest blue-to-red absorption ratios, the $a_{<ph>}(\lambda)$ spectra measured in NWW_{HT} ended up in a single cluster (Cluster 1, Figure 8b). These spectra showed very high proportions of both photosynthetic and photoprotective pigments and degradation products of chlorophyll *a* to [TChl *a*], very high $a^*_{ph}(440)$ and $a^*_{ph}(676)$ (section 3.1) and high "misclassified" percentage of diatoms (average of 71%) according to CHEMTAX. These samples are very likely dominated by *P. antarctica* (the main species of haptophytes in Antarctic waters) based on their $a_{<ph>}(\lambda)$ peak centered at 460 nm, indicative of the biomarker pigment 19′-hexanoyloxyfucoxanthin.

Cluster 2 grouped the $a_{<ph>}(\lambda)$ spectra with the greatest [Allo]/[TChl *a*], consistent with the highest mean percentage contribution of cryptophytes (~43%). Indeed, the shoulders at 460 and 490 nm, which are common to all the Cluster 2 spectra, resemble the absorption spectrum of the photoprotective pigment alloxanthin (Figure 8c). Cluster 3 is composed by $a_{<ph>}(\lambda)$ spectra with high proportion of the photosynthetic pigments [Hexa] and [Buta] and the photoprotective pigment [Diadi], in addition to equivalent contributions of diatom (~32%) and $dinof_2/diato_2$ (~36%) (Table 2 and Figure 8d). Cluster 4 is characterized by $a_{<ph>}(\lambda)$ spectra related to high contribution of [Diadi]/[TChl a] (mean of 0.073), that agreed to an absorption shoulder at 490 nm (Figure 8e). Clusters 1–4 comprised mostly $L_{>37\%}$ and $L_{37-10\%}$ samples (Table 2).

In agreement to an increasing package effect from Clusters 1 to 7, Clusters 5 to 7 comprised predominantly samples in $L_{<10\%}$ with high [PSC]/[TChl *a*] (Table 2). Cluster 6 gathered $a_{<ph>}(\lambda)$ spectra associated with high [Degr]/[TChl *a*], consistent with an absorption peak around 412 nm common to all spectra in that cluster, typical of degradation products of chlorophyll *a*. The presence of degradation products is in general related to grazing and senescent phytoplankton cells. The spectra in Cluster 6 were also related to a high proportion of the photoprotective pigment diatoxanthin, [Diato]/[TChl *a*], and the highest proportions (average of 0.052) of the photoprotective pigment β-carotene, [β-car]/[TChl *a*] (except for the highest [β-car]/[TChl *a*] of Cluster 1), even though most of those spectra (57 of 61) were found in $L_{<10\%}$. However, no shoulder indicative of β-carotene was revealed in the Cluster 7 spectra. Cluster 7 grouped samples with the highest [Fuco]/[TChl *a*] and lowest $a^*_{ph}(440)$ and $a^*_{ph}(676)$ (Table 2). This is an important result since similar values of $a^*_{ph}(\lambda)$ were generally observed along the vertical (section 3.1), while the clustering analysis gathered $a_{<ph>}(\lambda)$ spectra associated with $a^*_{ph}(440)$ and $a^*_{ph}(676)$ consistently lower in a single cluster. Note that the similar ranges of $a^*_{ph}(\lambda)$ for the majority of clusters (Clusters 2–6) agrees with the notion that variations in $a^*_{ph}(\lambda)$ did not show any clear pattern with S_f (Figure 7e). Therefore, variations in $a^*_{ph}(\lambda)$ are not necessarily accompanied by variations in the package effect in Antarctic waters.

The ratio [Fuco]/[TChl *a*] increased from Clusters 2 to 7, which gathered spectra associated with a dominance of diatoms in depth, according to CHEMTAX (average of ~65%) (Table 2). Nonetheless, as no microscopic information is available, we cannot rule out the possibility that the increase in [Fuco]/[TChl *a*] at depth results from an increase in intracellular fucoxanthin content. Previous observations in the Antarctic Peninsula of a general dominance of diatoms in the mixed layer at shallower depths [*Mendes et al.*, 2012] reinforce the suggestion that increasing [Fuco]/[TChl *a*] in depth reveals an increase of fucoxanthin relative to [TChl *a*] rather than a real increase in the relative contribution of diatoms to the total phytoplankton

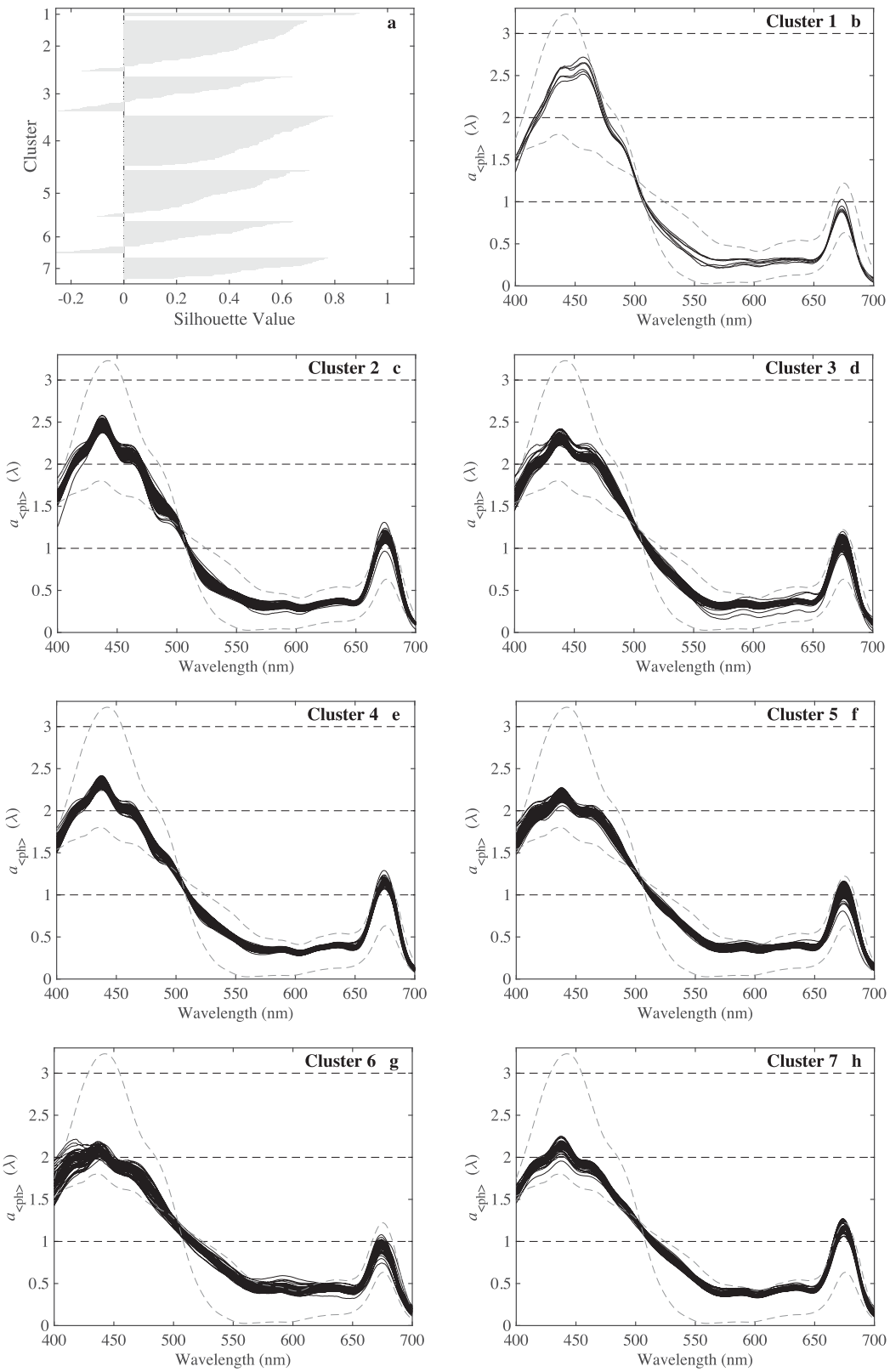

Figure 8. (a) Silhouette plot that displays values ranged from −1 to +1. A high silhouette value indicates that a sample is well matched to its own cluster, and poorly matched to neighboring clusters. (b–h) Spectra of phytoplankton absorption coefficient normalized to its mean value computed on the basis of all spectral values between 400 and 700 nm, $a_{<ph>}(\lambda)$, no unit, showed according to the clusters created on the basis of $a_{<ph>}(\lambda)$ through the *k*-means algorithm. The vectors of picophytoplankton and microphytoplankton spectral absorption used in the S_f model are also shown for comparison as dashed lines.

Table 2. Mean and Coefficient of Variation, CV (Standard Deviation Divided by Mean) Times 100 (i.e., in Percentage) of Selected Variables for Each of the Seven $a_{<ph>}(\lambda)$-Based Clusters[a]

	Cluster 1		Cluster 2		Cluster 3		Cluster 4		Cluster 5		Cluster 6		Cluster 7	
	Mean	CV (%)	Mean	CV (%)	Mean	CV (%)	Mean	CV (%)	Mean	CV (%)	Mean	CV (%)	Mean	CV (%)
[Fuco]/[TChl *a*]	0.448	6.0	0.209	39.6	0.352	17.2	0.292	26.4	0.375	18.3	0.389	15.2	0.430	17.2
[Hexa]/[TChl *a*]	0.287	8.7	0.099	47.0	0.164	33.7	0.090	33.0	0.140	35.9	0.137	38.0	0.065	46.8
[Buta]/[TChl *a*]	0.035	9.2	0.046	53.9	0.073	47.4	0.058	40.8	0.082	34.4	**0.087**	42.4	0.037	57.6
[Diadi]/[TChl *a*]	0.312	13.2	0.083	37.8	0.090	29.9	0.073	28.8	0.059	30.1	0.045	23.0	0.066	31.6
[Allo]/[TChl *a*]	0.013	39.5	0.146	52.3	0.032	93.9	0.077	56.5	0.023	93.7	0.016	91.2	0.023	99.4
[Diato]/[TChl *a*]	0.019	34.7	0.010	53.8	0.010	46.3	0.007	47.6	0.008	35.1	0.011	43.3	0.009	42.4
[β-car]/[TChl *a*]	0.171	15.3	0.017	63.1	0.030	75.4	0.018	58.1	0.046	70.5	0.097	51.6	0.022	76.2
$a^*_{ph}(440)$	0.085	11.7	0.046	21.1	0.045	28.7	0.041	19.7	0.044	18.9	0.050	23.8	0.031	27.4
$a^*_{ph}(676)$	0.031	8.8	0.022	20.5	0.021	25.1	0.020	19.0	0.021	16.2	0.022	20.8	0.017	24.2
[PSC]/[TChl *a*]	0.781	2.8	0.367	37.1	0.609	16.4	0.459	20.9	0.617	14.1	0.629	12.9	0.542	8.9
[PPC]/[TChl *a*]	0.384	11.8	0.272	23.4	0.162	22.9	0.188	22.2	0.119	20.6	0.103	19.6	0.124	24.3
$f_{diato/dinof}$	0.614	5.3	0.347	36.9	0.556	19.2	0.494	23.8	0.581	18.9	0.573	19.1	0.745	17.5
[Degr]/[TChl *a*]	0.190	17.9	0.050	32.0	0.057	42.9	0.049	33.9	0.082	49.9	0.104	45.7	0.057	36.4
%Diato	70.71	10.1	15.55	90.1	32.62	56.5	30.53	61.0	35.89	50.7	41.07	51.9	65.48	25.4
%dinof$_2$/diato$_2$	3.86	68.6	28.38	61.1	36.74	67.2	33.12	52.2	39.87	54.2	36.17	65.8	15.66	75.8
%Crypto	1.71	169.0	43.22	48.5	9.48	94.7	25.31	54.5	8.53	96.0	6.97	88.9	8.61	100.8
%*Phaeo*	20.67	11.9	7.01	104.3	15.71	69.0	5.88	98.3	10.50	81.7	10.28	66.2	7.65	54.8
S_f	0.56	7.8	0.41	5.7	0.37	9.1	0.34	6.8	0.30	7.3	0.23	15.9	0.22	14.9
N in $Z_{37\%}$	4		56		33		36		9		2		13	
N in $Z_{37-10\%}$	2		32		13		56		14		0		8	
N in $Z_{<10\%}$	0		10		21		33		64		57		21	
N in 2013	0		54		37		41		52		39		23	
N in 2014	6		44		30		54		36		22		19	
Total *N*	6		98		67		95		88		61		42	

[a]The number of spectra grouped within each cluster in $L_{>37\%}$, $L_{37-10\%}$, and $L_{<10\%}$, for each sampling year and total number of spectra for each cluster is also shown. Specifically, we consider the ratios of the main photosynthetic and photoprotective pigments that contributed to [PSC] and [PPC], i.e., fucoxanthin, [Fuco], 19′-hexanoyloxyfucoxanthin, [Hexa], 19′-butanoyloxyfucoxanthin, [Buta], diadinoxanthin, [Diadi], alloxanthin, [Allo], diatoxanthin, [Diato], and β-carotene, [β-car] to [TChl *a*]; $a^*_{ph}(440)$, $a^*_{ph}(676)$, [PSC]/[TChl *a*], [PPC]/[TChl *a*]; the sum of degradation products of chlorophyll *a* (chlorophyllide *a*, pheophytin *a* and pheophorbide *a*), [Degr] to [TChl *a*]; the percentage of the four main taxonomic groups of phytoplankton estimated through CHEMTAX, diatoms, %Diato, dinof$_2$/diato$_2$, %Dino$_2$/Diato$_2$, cryptophytes, %Crypto, and *Phaeocystis antarctica*, %*Phaeo*; and S_f.

biomass. This aspect emphasizes the importance of microscopic information in association to pigment data when making inferences about phytoplankton taxonomy, mainly along the vertical axis where pigment ratios vary with light and/or nutrient availability [see *Rodriguez et al.*, 2002; *Mendes et al.*, 2012]. High [Fuco]/[TChl *a*] ratios in $L_{<10\%}$ were associated with the $a_{ph}(\lambda)$ spectra with the strongest package effect found in this study (Figure 8h). Gradual changes in the contribution of other taxonomic groups from Clusters 1 to 7 were less evident (Table 2). Excluding the few $a_{<ph>}(\lambda)$ spectra measured in NWW$_{HT}$ (away from the Antarctic Peninsula) that showed the highest S_f (weakest package effect, Cluster 1), the weakest package effect was found in $L_{>37\%}$, when cryptophytes, identified by a high proportion of alloxanthin, were dominant (Cluster 2).

In summary, we illustrate the capacity of a clustering analysis based on the $a_{<ph>}(\lambda)$ spectra to identify a regular increase in the package effect, mainly in association with a regular increase in fucoxanthin and decrease of photoprotective pigments relative to [TChl *a*] (Figure 9). A similar degree of variability has been shown by cluster analysis on the bio-optical and photosynthetic properties of phytoplankton in the Argentine Sea [*Segura et al.*, 2013]. The cluster analysis reinforced that variations in the package effect are not reflected in $a^*_{ph}(\lambda)$, as seen from similar values of $a^*_{ph}(\lambda)$ from Clusters 2 to 6. The exception was the two extreme spectral shapes (Clusters 1 and 7, Figure 9d), which were associated with the highest and lowest values of $a^*_{ph}(\lambda)$ (Figure 9a). This approach can be useful to classify the phytoplankton assemblages in Antarctic waters according to different degrees of package effect, each one related to a specific pigment composition. The applicability of the S_f retrieval from multispectral satellite data [*Ciotti and Bricaud*, 2006; *Bricaud et al.*, 2012] is of special interest given the logistical difficulties to perform field samplings in the Southern Ocean. We also emphasize the need for increased efforts aiming at detailed characterization of the contribution of pigment composition to drive the variability in the phytoplankton absorption in different regions of Antarctic waters. This should improve the comprehension of the reasons for deviations in the global bio-optical algorithms when applied to the Southern Ocean. Investigations on the coherence

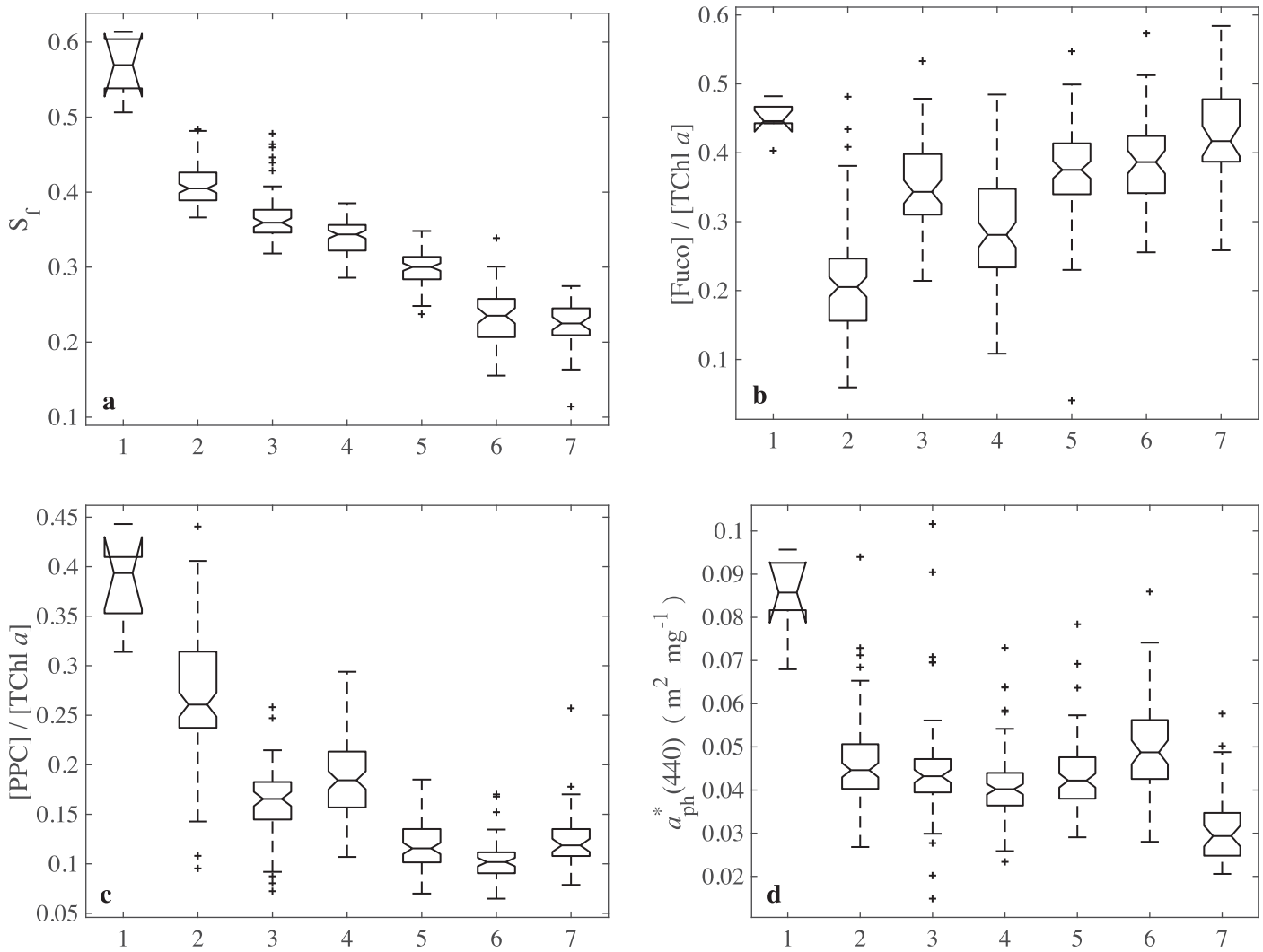

Figure 9. Boxplots of (a) the proxy of package effect, S_f; the proportions of (b) fucoxanthin to chlorophyll *a*, [Fuco]/[TChl *a*] and (c) photoprotective pigments to [TChl *a*], [PPC]/[TChl *a*] and (d) the chl *a*-specific absorption coefficient of phytoplankton at 440 nm, $a^*_{ph}(440)$ for the seven $a_{<ph>}(\lambda)$-based clusters. On each box, the central mark is the median and the edges of the box are the 25th and 75th percentiles. The whiskers extend to the most extreme data points that are not considered outliers. The outliers are plotted individually as crosses. The interval endpoints are the extremes of the notches. Whisker absences for Cluster 1 indicate lack of values outside the interval of lower or upper quantiles.

between S_f and chlorophyll *a* and accessory pigments in other regions worldwide would also provide insights into the sources of variability in the spectral shape of phytoplankton absorption, such as regional differences in pigment composition and cell size for a similar phytoplankton biomass.

4. Conclusions

The coefficient $a^*_{ph}(\lambda)$ did not vary inversely to chlorophyll *a* concentration. Despite the acknowledged importance of accessory pigments in driving the variability in the phytoplankton spectral absorption, mainly in the blue wavelengths, their effects were not clearly identified in $a^*_{ph}(\lambda)$. This is an important result because lower and higher $a^*_{ph}(\lambda)$ are generally attributed to larger and smaller pigment packaging and cell size, and to lower and higher relative importance of accessory pigments, respectively. Variations in the proportion of accessory pigments to chlorophyll *a* were easily discernible in absorption ratios ($a_{ph}(440)/a_{ph}(490)$ for photosynthetic and $a_{ph}(460)/a_{ph}(490)$ for photoprotective pigments).

We described variations in the package effect in Antarctica waters based solely on the phytoplankton absorption spectrum, independently of chlorophyll *a* concentration, with a simple interpretation. S_f varies within a continuum of spectrum flatness, i.e., from 0 (the strongest package effect) to 1 (the weakest

package effect). We provided a means to delineate distinct degrees of package effect through different ranges of S_f as revealed in a decreasing continuum of spectral flatness ordered by a cluster analysis on the phytoplankton absorption spectrum normalized by its mean value computed between 400 and 700 nm. A regular increase in the degree of package effect was mainly associated with a regular increase of fucoxanthin and decrease of photoprotective pigments relative to chlorophyll *a*.

Appendix A: Determination of the Phytoplankton Cell Size With Chlorophyll *a* Fractionation

For 17 near surface samples (5 m), chlorophyll *a* size fractionation was performed to complement the taxonomic information of phytoplankton obtained from CHEMTAX. Five stations (average [TChl *a*] of 1.31 mg m^{-3}) and eight stations (average [TChl *a*] of 1.49 mg m^{-3}) were chosen in BS in 2013 and 2014, respectively, and four stations (average [TChl *a*] of 1.75 mg m^{-3}) in GS in 2014. A serial system of filtration was used. Each sample was firstly filtered onto a polycarbonate filter with pore size of 20 μm (GE Water & Process Technologies, 47 mm). The collected filtrate was subsequently filtered onto a polycarbonate filter with pore size of 2 μm (GE Water & Process Technologies, 47 mm). Finally, the collected filter was filtered onto a GF/F filter (Whatman) to retain the cells <2 μm. The first two filtrations were performed by gravity and the last one under low vacuum (<5 in Hg). The filtration by gravity minimizes the usual problems of filtration under vacuum, such as broken phytoplankton cells. This procedure yielded HPLC-derived chlorophyll *a* concentration, [Chl *a*], for the picophytoplankton (<2 μm), nanophytoplankton (2–20 μm), and microphytoplankton (>20 μm).

In 2013, picophytoplankton and nanophytoplankton contributions varied from 19 to 67% and 30 to 61% (average of 45% each), respectively, followed by a minimum microphytoplankton content, with contributions of 3–5%. A single sample with [Chl *a*] of 2.23 mg m^{-3} contained a moderate microphytoplankton proportion of 34%. In 2014, the four stations in GS showed equivalent contributions of picophytoplankton and nanophytoplankton (averages of 41 and 40%, respectively) and 2, 4, 15, and 54% of microphytoplankton contribution. The contribution of 54% was related to [Chl *a*] of 2.46 mg m^{-3}. In BS, the contribution of microphytoplankton was negligible, with percentages of 1–4%. The picophytoplankton and nanophytoplankton ranged from 12 to 62% and 32 to 87%, respectively. Interestingly, the second highest contribution of picophytoplankton (60%) was observed in association to the highest [Chl *a*] in samples for which the fractionated filtration was done (2.49 mg m^{-3}). An independent filtration system using low vacuum (<5 in Hg) performed fractionation of HPLC-derived chlorophyll *a* in 10 near surface samples in 2014, choosing different stations for the procedure described above, for the size fractions of <5 and >20 μm. For that, samples were passed throughout 5 and 20 μm meshes and the collected filtrate was subsequently filtered onto the GF/F filter. The results of this analysis confirmed the observations with filtration by gravity, as the <5 μm fraction massively dominated the samples, with percentages of 60–96% of [Chl *a*]. Figure 1a shows the increase of package effect of phytoplankton absorption (lower S_f) once the microphytoplankton fraction increases.

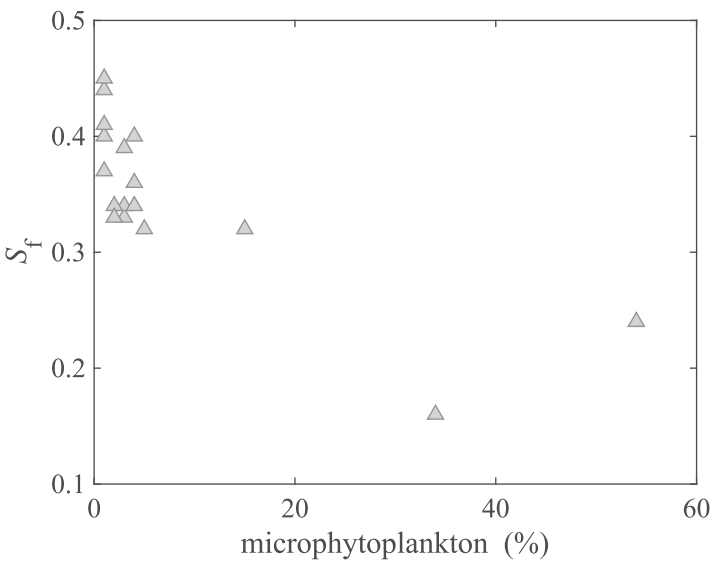

Figure A1. The proxy of package effect, S_f, as a function of percentage of microphytoplankton, for samples which chlorophyll *a* size fractionation was available. The correlation coefficient for the log-transformed data is $r = -0.83$, $p < 0.0001$, $N = 18$.

Part of the filter-fractionated picophytoplankton is possibly overestimated to some extent because the size of some cells that pass through a filter is determined by

their width rather than length [*Wright et al.*, 2009]. Even so, the contributions obtained from gravity filtration are average of duplicates, with results very close to each other. Therefore, picophytoplankton is an important component in our samples. This is a very interesting result as the most abundant groups estimated by CHEMTAX generally belong to nanophytoplankton (*P. antarctica*, cryptophytes, dinof$_2$/diato$_2$) and microphytoplankton (diatoms). In fact, some groups normally attributed to both size fractions can be true picoplanktonic cells, as observed by *Wright et al.* [2009] in the eastern Antarctic coast. Based on electron microscopy, the authors found that most organisms in a filter-derived picoplankton fraction were actually nanoeukaryotes and the proportion of autotrophs <2 μm was exceedingly small, although they used vacuum filtration (differently to our procedure). We are confident that most of the phytoplankton in our surveys near surface comprises picophytoplankton and nanophytoplankton (including very small cells in this range) although the proportion of each fraction for most of the samples, for which there is no chlorophyll *a* fractionation, remains unknown.

This is an important aspect [see also *Lutz et al.*, 2016] and cautions the use of diagnostic pigments to derive phytoplankton size proportions [*Vidussi et al.*, 2001; *Uitz et al.*, 2006] and dominant cell size [*Bricaud et al.*, 2004] if previous knowledge of the studied region or additional information is not available. For instance, the very high proportion of diatoms in many of our samples was unreasonably associated with a great importance of microphytoplankton based on the use of diagnostic pigments as proposed by *Uitz et al.* [2006], assuming this taxonomic group belongs to the largest size of algal component. The opposite result is observed for the picophytoplankton contribution, for which the method based on diagnostic pigments yields very low contributions (average of $\sim$9%) compared with the fractionation data. Comparison of size fractionations and diagnostic pigment approaches of phytoplankton can also be found elsewhere [e.g., *Varela et al.*, 2002; *Uitz et al.*, 2009; *Brewin et al.*, 2015]. Our finding of diatom-containing picoplankton in our samples may partially support the differences in the relationship between diagnostic pigments and chlorophyll *a* concentration [*Hirata et al.*, 2011] for the Southern Ocean compared to global relationships [*Soppa et al.*, 2014].

Appendix B: Chlorophyll-Specific Absorption Coefficient as a Function of Total Chlorophyll *a*

Variations in $a^*_{ph}(440)$ are attributed to changes in algal cell size, chlorophyll *a* content per cell, and the presence of carotenoids that absorb in the blue spectral region, while variations in $a^*_{ph}(676)$ can be mostly attributed to changes in chlorophyll *a* content per cell and cell size. To first order, the influence of pigment packaging can be assessed in the red absorption band of chlorophyll *a*. Figure B1 reveals that, despite the general pattern of $a^*_{ph}(\lambda)$ to decrease with increasing [TChl *a*], [TChl *a*] explained only 31 and 22% of

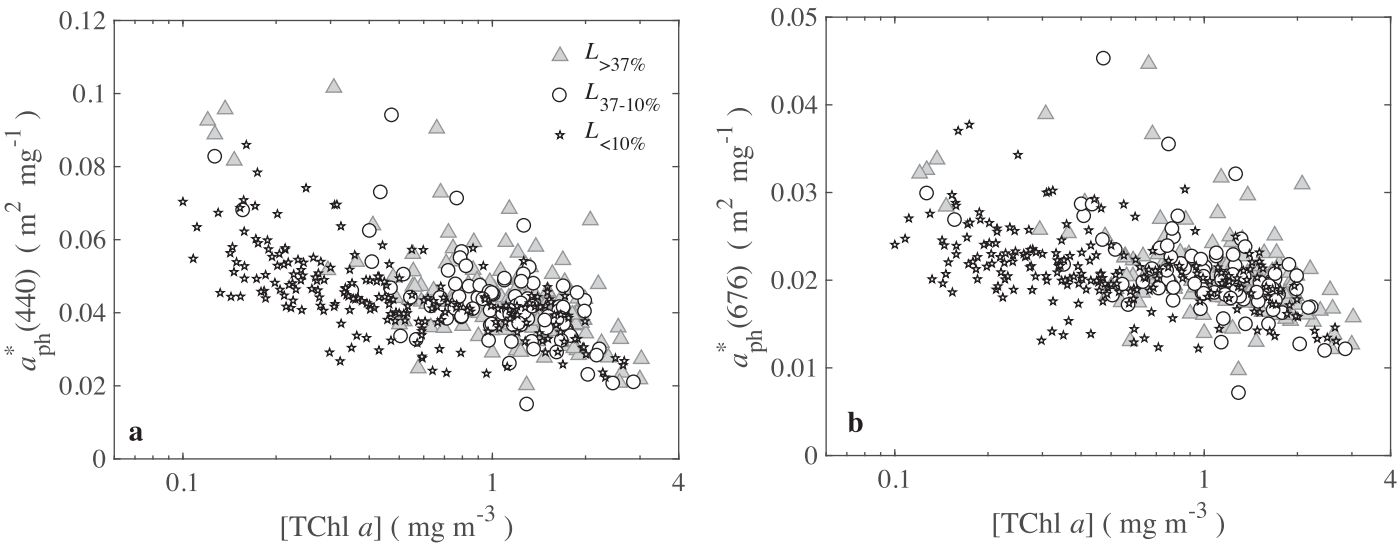

Figure B1. The chlorophyll-specific absorption coefficient of phytoplankton, $a^*_{ph}(\lambda)$ at (a) 440 nm and (b) 676 nm, as a function of total chlorophyll *a* concentration, [TChl *a*], in $L_{37\%}$, $L_{37-10\%}$ and $L_{<10\%}$.The regression formula and the best fit parameters for this study are $a^*_{ph}(440) = 0.041$ [TChl *a*]$^{-0.187}$ ($R^2 = 0.31$; $p < 0.00001$; $N = 455$) and $a^*_{ph}(676) = 0.020$ [TChl *a*]$^{-0.124}$ ($R^2 = 0.22$; $p < 0.00001$; $N = 455$).

variations in $a^*_{ph}(440)$ and $a^*_{ph}(676)$, respectively. This poor correlation has implications when attempting to derive chlorophyll *a* concentration from phytoplankton absorption using ocean color models based on $a^*_{ph}(\lambda)$ [e.g., *Dall'Olmo et al.*, 2005] in Antarctic waters.

Acknowledgments
This work is part of a multidisciplinary program under the GOAL (Brazilian High Latitudes Oceanography Group) activities in the Brazilian Antarctic Program (PROANTAR). Financial support was provided by CNPq (National Council for Research and Development) for the POLARCANION (CNPq grant 556848/2009–8) and PRO-OASIS (CNPq grant 565040/2010–3) projects. Amabile Ferreira was supported by FAPESP (Research Support Foundation of the State of São Paulo, FAPESP, grants 2013/16957–2 and 2016/01601–6). C. R. B. Mendes acknowledges financial support from the CAPES Foundation. Áurea M. Ciotti thanks CNPq for the research fellowship (PQ 310985/2013–7). The authors thank the crew of the Polar Vessel "Almirante Maximiano" of the Brazilian Navy and several investigations on the cruises for assistance. We thank Bianca Tocci and Maria Fernanda C. Giannini for help during field work. This research is a contribution of the NP-BioMar, University of São Paulo. We acknowledge Shubha Sathyendranath and an anonymous reviewer for their valuable contributions which have greatly improved the manuscript. The data set used in this work can be accessed in https://doi.pangaea.de/10.1594/PANGAEA.879657.

References

Alderkamp, A. C., H. W. J. De Baar, R. J. W. Visser, and K. R. Arrigo (2010), Can photoinhibition control phytoplankton abundance in deeply mixed water columns of the Southern Ocean?, *Limnol Oceanogr.*, *55*, 1248−1264, doi:10.4319/lo.2010.55.3.1248.

Alderkamp, A. C., V. Garcon, H. J. W. De Baar, and K. R. Arrigo (2011), Short-term photoacclimation effects on photoinhibition of phytoplankton in the Drake passage (Southern Ocean), *Deep Sea Res., Part I*, *58*, 943−955, doi:10.1016/j.dsr.2011.07.001.

Alderkamp, A. C., M. M. Mills, G. L. van Dijken, and K. R. Arrigo (2013), Photoacclimation and non photochemical quenching under in situ irradiance in natural phytoplankton assemblages from the Amundsen Sea, Antarctica, *Mar. Ecol. Prog. Ser.*, *475*, 15−34, doi:10.3354/meps10097.

Arrigo, K. R., D. H. Robinson, D. L. Worthen, B. Schieber, and M. P. Lizotte (1998), Bio optical properties of the southwestern Ross Sea, *J. Geophys. Res.*, *103*, 21,683–21,695, doi:10.1029/98JC02157.

Brewin, R. J. W., S. Sathyendranath, T. Jackson, R. Barlow, V. Brotas, R. Airs, and T. Lamont (2015), Influence of light in the mixed layer on the parameters of a three-component model of phytoplankton size structure, *Remote Sens. Environ.*, *168*, 437–450, doi:10.1016/j.rse.2015.07.004.

Bricaud, A., M. Babin, A. Morel, and H. Claustre (1995), Variability in the chlorophyll specific absorption coefficients of natural phytoplankton: Analysis and parameterization, *J. Geophys. Res.*, *100*, 13,321–13,332, doi:10.1029/95JC00463.

Bricaud, A., H. Claustre, J. Ras, and K. Oubelkheir (2004), Natural variability of phytoplankton absorption in oceanic waters: influence of the size structure of algal populations, *J. Geophys. Res.*, *109*, C11010, doi:10.1029/2004JC002419.

Bricaud, A., A. M. Ciotti, and B. Gentili (2012), Spatial-temporal variations in phytoplankton size and colored detrital matter absorption at global and regional scales, as derived from twelve years of SeaWiFS data (1998–2009), *Global Biogeochem. Cycles*, *26*, GB1010, doi:10.1029/2010GB003952.

Cheah, W., A. McMinn, F. B. Griffiths, K. J. Westwood, S. W. Wright, and L. A. Cleme (2013), Response of phytoplankton photophysiology to varying environmental conditions in the sub-Antarctic and Polar Frontal Zone, *PLoS ONE*, *8*(8), e72165, doi:10.1371/journal.pone.0072165.

Ciotti, A. M., and A. Bricaud (2006), Retrievals of a size parameter for phytoplankton and light absorption by colored detrital matter from water-leaving radiances at SeaWiFS channels in a continental shelf region off Brazil, *Limnol. Oceanogr. Methods*, *4*, 237–253, doi:10.4319/lom.2006.4.237.

Ciotti, A. M., M. R. Lewis, and J. J. Cullen (2002), Assessment of the relationships between dominant cell size in natural phytoplankton communities and the spectral shape of the absorption coefficient, *Limnol. Oceanogr.*, *47*, 404–417.

Dall'Olmo, G., A. A. Gitelson, D. C. Rundquist, B. Leavitt, T. Barrow, and J. Holz (2005), Assessing the potential of SeaWiFS and MODIS for estimating chlorophyll concentration in turbid productive waters using red and near-infrared bands, *Remote Sens. Environ.*, *96*, 176–87, doi:10.1016/j.rse.2005.02.007.

Dierssen, H. M., and R. C. Smith (2000), Bio-optical properties and remote sensing ocean color algorithms for Antarctic Peninsula waters, *J. Geophys. Res.*, *105*, 26,301–26,312, doi:10.1029/1999JC000296.

Duysens, L. N. M. (1956), The flattening of the absorption spectrum of suspensions as compared to that of solutions, *Biochim. Biophys. Acta*, *19*, 1–12.

Garcia, C. A. E., V. M. T. Garcia, and C. McClain (2005), Evaluation of SeaWiFS chlorophyll algorithms in the Southwestern Atlantic and Southern Oceans, *Remote Sens. Environ.*, *95*, 125–137, doi:10.1016/j.rse.2004.12.006.

García-Muñoz, C., L. M. Lubián, C. M. García, A. Marrero-Díaz, P. Sangrà, and M. Vernet (2013), A mesoscale study of phytoplankton assemblages around the South Shetland Islands (Antarctica), *Polar Biol.*, *36*, 1107−1123, doi:10.1007/s00300-013-1333-5.

García-Muñoz, C., C. Sobrino, L. Lubián, C. García, S. Martínez-García, and P. Sangrà (2014), Factors controlling phytoplankton physiological state around the South Shetland Islands (Antarctica), *Mar. Ecol. Prog. Ser.*, *498*, 55–71, doi:10.3354/meps10616.

Garver, S. A., D. A. Siegel, and B. G. Mitchell (1994), Variability in near surface particulate absorption spectra: What can a satellite ocean color imager see?, *Limnol. Oceanogr.*, *39*, 1349–1367.

Gonçalves-Araújo, R., M. S. de Souza, V. M. Tavano, and C. A. E. Garcia (2015), Influence of oceanographic features on spatial land interannual variability of phytoplankton in the Bransfield Strait, Antarctica, *J. Mar. Syst.*, *142*, 1–15, doi:10.1016/j.jmarsys.2014.09.007.

Gordon, H. R., and W. R. McCluney (1975), Estimation of the depth of sunlight penetration in the sea for remote sensing, *Appl. Opt.*, *14*(2), 413–416.

Gordon, H. R., and A. Morel (1983), *Remote Assessment of Ocean Color for Interpretation of Satellite Visible Imagery: A Review*, 114 pp., Springer, New York.

Hirata, T., et al. (2011), Synoptic relationships between surface chlorophyll-*a* and diagnostic pigments specific to phytoplankton functional types, *Biogeosciences*, *8*, 311–327, doi:10.5194/bg-8-311-2011.

Hoepffner, N., and S. Sathyendranath (1991), Effect of pigment composition on absorption properties of phytoplankton, *Mar. Ecol. Prog. Ser.*, *73*, 11–23, doi:10.3354/meps073011

Jeffrey, S. W., R. F. C. Mantoura, and S. W. Wright (1997), *Phytoplankton Pigments in Oceanography: Guidelines to Modern Methods*, UNESCO, Paris.

Johnson, R., P. G. Strutton, S. W. Wright, A. McMinn, and K. M. Meiners (2013), Three improved satellite chlorophyll algorithms for the Southern Ocean, *J. Geophys. Res. Oceans*, *118*, 3694–3703, doi:10.1002/jgrc.20270.

Kahru, M., and B. G. Mitchell (2010), Blending of ocean colour algorithms applied to the Southern Ocean, *Remote Sens. Lett.*, *1*(2), 119–124, doi:10.1080/01431160903547940.

Kang, S. H., J. S. Kang, S. Lee, K. H. Chung, D. Kim, and M. G. Park (2001), Antarctic phytoplankton assemblages in the marginal ice zone of the northwestern Weddell Sea, *J. Plankton Res.*, *23*, 333–352, doi:10.1093/plankt/23.4.333.

Kaufmann, L., and P. J. Rousseeuw (1990), *Finding Groups in Data*, John Wiley, New York.

Kozlowski, W. A., D. Deutschman, I. Garibotti, C. Trees, and M. Vernet (2011), An evaluation of the application of CHEMTAX to Antarctic coastal pigment data, *Deep Sea Res., Part I*, *58*, 350–364, doi:10.1016/j.dsr.2011.01.008.

Lubac, B., and H. Loisel (2007), Variability and classification of remote sensing reflectance spectra in the eastern English Channel and southern North Sea, *Remote Sens. Environ.*, *110*, 45–58, doi:10.1016/j.rse.2007.02.012.

Lutz, V., R. Frouin, R. Negri, R. Silva, M. Ponpeu, N. Rudorff, A. Cabral, A. Dogliotti, and G. Martinez (2016), Bio-optical characteristics along the Straits of Magallanes, *Cont. Shelf Res.*, *119*, 56–67, doi:10.1016/j.csr.2016.03.008.

Mackey, M. D., D. J. Mackey, H. W. Higgins, and S. W. Wright (1996), CHEMTAX—A program for estimating class abundances from chemical markers: Application to HPLC measurements of phytoplankton, *Mar. Ecol. Prog. Ser.*, *144*, 265–283, doi:10.3354/meps144265.

Marrari, M., C. Hu, and K. Daly (2006), Validation of SeaWiFS chlorophyll *a* concentrations in the Southern Ocean: A revisit, *Remote Sens. Environ.*, *105*(4), 367–375, doi:10.1016/j.rse.2006.07.008.

Mendes, C. R., P. Cartaxana, and V. Brotas (2007), HPLC determination of phytoplankton and microphytobenthos pigments: Comparing resolution and sensitivity of a C18 and a C8 method, *Limnol. Oceanogr. Methods*, *5*, 363–370, doi:10.4319/lom.2007.5.363.

Mendes, C. R. B., M. S. de Souza, V. M. T. Garcia, M. C. Leal, V. Brotas, and C. A. E. Garcia (2012), Dynamics of phytoplankton communities during late summer around the tip of the Antarctic Peninsula, *Deep Sea Res., Part I*, *65*, 1–14, doi:10.1016/j.dsr.2012.03.002.

Mendes, C. R. B., V. M. Tavano, M. C. Leal, M. S. de Souza, V. Brotas, and C. A. E. Garcia (2013), Shifts in the dominance between diatoms and cryptophytes during three late summers in the Bransfield Strait (Antarctic Peninsula), *Polar Biol.*, *36*, 537–547, doi:10.1007/s00300-012-1282-4.

Mendes, C. R. B., V. M. Tavano, T. S. Dotto, R. Kerr, M. S. de Souza, and C. A. E. Garcia (2017), New insights on the dominance of cryptophytes in Antarctic coastal waters: A case study in Gerlache Strait, *Deep Sea Res., Part II*, doi:10.1016/j.dsr2.2017.02.010, in press.

Mitchell, B. G. (1992), Predictive bio-optical relationships for polar oceans and marginal ice zones, *J. Mar. Syst.*, *3*, 91–105.

Mitchell, B. G., and O. Holm-Hansen (1991), Bio-optical properties of Antarctic Peninsula waters: Differentiation from temperate ocean models, *Deep Sea Res., Part I*, *38*(8–9), 1009–1028.

Neale, P. J., W. H. Jeffrey, C. Sobrino, J. D. Pakulski, J. D. Phillips-Kress, A. J. Baldwin, L. A. Franklin, and H. Kim (2009), Inhibition of phytoplankton and bacterial productivity by solar radiation in the Ross Sea Polynya, in *Smithsonian at the Poles. Contributions to International Polar Year Science*, edited by I. Krupnik, M. Lang, and S. Miller, pp. 299–308, Smithson. Press, Washington, D. C.

Neale, P. J., C. Sobrino, and A. E. Gargett (2012), Vertical mixing and the effects of solar radiation on photosystem II electron transport by phytoplankton in the Ross Sea Polynya, *Deep Sea Res., Part I*, *63*, 118–132, doi:10.1016/j.dsr.2012.01.011.

Reynolds, R. A., D. Stramski, and B. G. Mitchell (2001), A chlorophyll-dependent semi analytical reflectance model derived from field measurements of absorption and backscattering coefficients within the Southern Ocean, *J. Geophys. Res.*, *106*, 7125–7138, doi:10.1029/1999JC000311.

Rodriguez, F., M. Varela, and M. Zapata (2002), Phytoplankton assemblages in the Gerlache and Bransfield Straits (Antarctic Peninsula) determined by light microscopy and CHEMTAX analysis of HPLC pigment data, *Deep Sea Res., Part II*, *49*, 723–747, doi:10.1016/S0967-0645(01)00121-7.

Russo, A. D. P. G., M. S. de Souza, C. F. B. Mendes, B. Jesus, V. M. Tavano, and C. A. E. Garcia (2015), Photophysiological effects of Fe concentration gradients on diatom-dominated phytoplankton assemblages in the Antarctic Peninsula region, *J. Exp. Mar. Biol. Ecol.*, *466*, 49–58, doi:10.1016/j.jembe.2015.02.002.

Sathyendranath, S., V. Stuart, T. Plat, H. Bouman, O. Ulloa, and H. Maass (2005), Remote sensing of ocean colour: Towards algorithms for retrieval of pigment composition, *Indian J. Mar. Sci.*, *34*(4), 333–340.

Segura, V., V. A. Lutz, A. Dogliotti, R. J. Silva, R. M. Negri, R. Akselman, and H. Benavides (2013), Phytoplankton types and primary production in the Argentine Sea, *Mar. Ecol. Prog. Ser.*, *491*, 15–31, doi:10.3354/meps10461.

Soppa, M. A., T. Hirata, S. Brenner, T. Dinter, I. Peeken, S. Wiegmann, and A. Bracher (2014), Global retrieval of diatoms abundance based on phytoplankton pigments and satellite, *Remote Sens.*, *6*, 10,089–10,106, doi:10.3390/rs61010089.

Sosik, H., M. Vernet, and B. G. Mitchell (1992), RACER 3: A comparison of particulate absorption properties between high- and mid-latitude surface waters, *Antarct. J. U.S.*, *27*, 162–164.

Stambler, N. (2003), Primary production, light absorption and quantum yields of phytoplankton from the Bellingshausen and Amundsen Seas (Antarctica), *Polar Biol.*, *26*, 438–451, doi:10.1007/s00300-003-0508-x.

Stambler, N., C. Lovengreen, and M. M. Tilzer (1997), The underwater light field in the Bellingshausen and Amundsen Seas (Antarctica), *Hydrobiologia*, *344*, 41–56.

Szeto, M., P. J. Werdell, T. S. Moore, and J. W. Campbell (2011), Are the worlds oceans optically different?, *J. Geophys. Res.*, *116*, C00H04, doi:10.1029/2011JC007230.

Tassan, S., and G. M. Ferrari (1995), An alternative approach to absorption measurements of aquatic particles retained on filters, *Limnol. Oceanogr.*, *40*, 1358–1368.

Tassan, S., G. M. Ferrari, A. Bricaud, and M. Babin (2000), Variability of the amplification factor of light absorption by filter-retained aquatic particles in the coastal environment, *J. Plankton Res.*, *22*, 659–668.

Taylor, B. B., E. Torrecila, A. Bernhardt, M. H. Taylor, I. Peeken, R. Roettgers, and A. Bracher (2011), Bio-optical provinces in the eastern Atlantic Ocean and their biogeographical relevance, *Biogeosciences*, *8*, 3609–3629, doi:10.5194/bgd-8-7165-2011.

Torrecilla, E., D. Stramski, R. A. Reynolds, E. Millan-Nunez, and J. Piera (2011), Cluster analysis of hyperspectral optical data for discriminating phytoplankton pigment assemblages in the open ocean, *Remote Sens. Environ.*, *115*, 2578–2593, doi:10.1016/j.rse.2011.05.014.

Trees, C. C., D. K. Clark, R. R. Bidigare, M. E. Ondrusek, and J. L. Mueller (2000), Accessory pigments versus chlorophyll *a* concentrations within the euphotic zone: A ubiquitous relationship, *Limnol. Oceanogr.*, *45*, 1130–1143, doi:10.4319/lo.2000.45.5.1130.

Uitz, J., H. Claustre, A. Morel, and S. B. Hooker (2006), Vertical distribution of phytoplankton communities in open ocean: An assessment based on surface chlorophyll, *J. Geophys. Res.*, *111*, C08005, doi:10.1029/2005JC003207.

Uitz, J., H. Claustre, F. B. Griffiths, J. Ras, N. Garcia, and V. Sandroni (2009), A phytoplankton class-specific primary production model applied to the Kerguelen islands region (Southern Ocean), *Deep Sea Res., Part I*, *56*(4), 541–560, doi:10.1016/j.dsr.2008.11.006.

Uitz, J., D. Stramski, R. A. Reynolds, and J. Dubranna (2015), Assessing phytoplankton community composition from hyperspectral measurements of phytoplankton absorption coefficient and remote-sensing reflectance in open-ocean environments, *Remote Sens. Environ.*, *171*, 58–74, doi:10.1016/j.rse.2015.09.027.

Van de Poll, W. H., P. J. Janknegt, M. A. van Leeuwe, R. J. W. Visser, and A. G. J. Buma (2009), Does ultraviolet radiation affect the xanthophyll cycle in marine phytoplankton?, *Photochem. Photobiol. Sci.*, *8*, 1295–1301.

Van Leeuwe, M. A., B. Van Sikkelerus, W. W. C. Gieskes, and J. Stefels (2005), Taxon specific differences in photoacclimation to fluctuating irradiance in an Antarctic diatom and a green flagellate, *Mar. Ecol. Prog. Ser.*, *288*, 9–19.

Varela, M., E. Fernandez, and P. Serret (2002), Size-fractionated phytoplankton biomass and primary production in the Gerlache and south Bransfield Straits (Antarctic Peninsula) in Austral summer 1995–1996, *Deep Sea Res., Part II*, *49*, 749–768.

Vidussi, F., H. Claustre, B. B. Manca, A. Luchetta, and J. C. Marty (2001), Phytoplankton pigment distribution in relation to upper thermocline circulation in the eastern Mediterranean Sea during winter, *J. Geophys. Res.*, *106*, 19,939–19,956, doi:10.1029/1999JC000308.

Wright, S. W., and S. W. Jeffrey (2006), Pigment markers for phytoplankton production, in *Marine Organic Matter: Biomarkers, Isotopes and DNA*, edited by J. K. Volkmann, pp. 71–104, Spring, Berlin.

Wright, S. W., A. Ishikawa, H. J. Marchant, A. T. Davidson, R. L. van der Enden, and G. V. Nash (2009), Composition and significance of picophytoplankton in Antarctic water, *Polar. Biol.*, *32*, 797–808, doi:10.1007/s00300-009-0582-9.